A missense mutation in *PPP1R15B* causes a syndrome including diabetes, short stature and microcephaly

Baroj Abdulkarim[1,#], Marc Nicolino[2,3,4,#,*], Mariana Igoillo-Esteve[1], Mathilde Daures[5,6], Sophie Romero[5,6], Anne Philippi[5,6], Valérie Senée[5,6], Miguel Lopes[1], Daniel A. Cunha[1], Heather P. Harding[7], Céline Derbois[8], Nathalie Bendelac[2], Andrew T. Hattersley[9], Décio L. Eizirik[1], David Ron[7], Miriam Cnop[1,10,*,#], Cécile Julier[5,6,*,#]

[1]ULB Center for Diabetes Research, Université Libre de Bruxelles (ULB), Brussels, Belgium; [2]Hôpital Femme-Mère-Enfant, Division of Pediatric Endocrinology, Hospices Civils de Lyon, Lyon1 University, Lyon, France; [3]Inserm U870, Lyon, France; [4]Inserm CIC201, Lyon, France; [5]Inserm UMR-S 958, Faculté de Médecine Paris Diderot, Paris, France; [6]University Paris 7 Denis–Diderot, Paris, France; [7]Cambridge Institute for Medical Research (CIMR), University of Cambridge, and NIHR Cambridge Biomedical Research Centre, Cambridge, United Kingdom; [8]Institut de Génomique, Centre National de Génotypage (CNG), Commissariat à l'Energie Atomique et aux Energies Alternatives (CEA), Evry, France; [9]University of Exeter Medical School, University of Exeter, Exeter, United Kingdom; [10]Division of Endocrinology, Erasmus Hospital, Brussels, Belgium

# These authors contributed equally to this work

*Correspondence should be addressed to:

Marc Nicolino, Hôpital Femme-Mère-Enfant, Division of Pediatric Endocrinology, Hospices Civils de Lyon, 59 bd Pinel, 69677 Bron cedex, France; tel : +33 1 4 72 12 95 27, e-mail : marc.nicolino@chu-lyon.fr; Miriam Cnop, ULB Center for Diabetes Research, Université Libre de Bruxelles (ULB), Route de Lennik 808, CP-618, 1070 Brussels, Belgium, tel: +32 2 555 6305; Fax: +32 2 555 6239, e-mail: mcnop@ulb.ac.be; Cécile Julier, Inserm UMR-S958, Faculté de Médecine Paris Diderot, 10 avenue de Verdun, 75010 Paris, France, tel: +33 1 57 27 85 43, FAX: +33 1 57 27 85 54, e-mail: cecile.julier@inserm.fr or

Running title: *PPP1R15B* mutation in a novel diabetes syndrome

Words count: 145 (abstract) and 4727 (main text). The manuscript contains 1 table and 6 figures.

Abstract

Dysregulated endoplasmic reticulum stress and phosphorylation of eukaryotic translation initiation factor 2α (eIF2α) are associated with pancreatic β-cell failure and diabetes. Here we report the first homozygous mutation in the *PPP1R15B* gene (also known as constitutive repressor of eIF2α phosphorylation, CReP), encoding the regulatory subunit of an eIF2α-specific phosphatase, in two siblings affected by a novel syndrome of diabetes of youth, with short stature, intellectual disability and microcephaly. The R658C mutation in PPP1R15B affects a conserved amino acid within the domain important for protein phosphatase 1 (PP1) binding. The R658C mutation decreases PP1 binding and eIF2α dephosphorylation, and results in β-cell apoptosis. Our findings support the concept that dysregulated eIF2α phosphorylation, whether decreased by mutation of the kinase (*EIF2AK3*) in Wolcott-Rallison syndrome or increased by mutation of the phosphatase (*PPP1R15B*), is deleterious to β-cells and other secretory tissues, resulting in diabetes associated with multi-system abnormalities.

The molecular mechanisms contributing to pancreatic β-cell dysfunction and apoptosis in diabetes remain poorly understood. Accumulating evidence suggests that endoplasmic reticulum (ER) stress and aspects of the response to it contribute to β-cell failure both in type 1 and type 2 diabetes (1-6). ER stress is defined as an imbalance between unfolded protein load in the ER and the organelle's functional capacity. This activates an ER stress response, also known as the unfolded protein response (UPR), which reduces protein load and increases ER folding capacity. The UPR is an adaptive response, particularly important for the survival of cells with a high secretory capacity such as pancreatic β-cells. The UPR is triggered by the activation of ER transmembrane proteins that sense the misfolded protein accumulation in the ER lumen and transduce the signal to the cytoplasm. One of the canonical ER stress transducers is protein kinase R-like endoplasmic reticulum kinase (PERK, encoded by *EIF2AK3*). PERK phosphorylates the eukaryotic translation initiation factor 2α (eIF2α) and attenuates protein translation to lessen the burden of the stressed ER (1;7). The effector pathway downstream of PERK is tightly regulated by eIF2α dephosphorylation carried out by a holophosphatase complex consisting of a common catalytic subunit, protein phosphatase 1 (PP1), and a substrate-specific regulatory subunit, PPP1R15. Two such regulatory subunits are known: the constitutive repressor of eIF2α phosphorylation (CReP), encoded by *PPP1R15B*, acts under basal conditions (8), while GADD34, encoded by *PPP1R15A*, is activated by eIF2α phosphorylation and feeds back negatively on PERK signaling to promote recovery of protein synthesis as the stress response wanes (9). The PERK pathway and its regulation are especially important for pancreatic β-cell function and survival (10-12). Homozygous mutations in *EIF2AK3* cause Wolcott-Rallison syndrome, a syndromic form of neonatal diabetes with epiphyseal dysplasia and growth retardation, and variable other manifestations including microcephaly (11;13), features mirrored in Perk knockout mice (14). Unmitigated ER stress contributes to β-cell demise in several other monogenic forms of

diabetes. Mutations in the insulin gene that disrupt pro-insulin folding cause severe β-cell ER stress and neonatal diabetes (15). Loss of the ER co-chaperone $p58^{IPK}$, due to *DNAJC3* mutations, leads to a syndrome with young onset diabetes (16).

Here we report on a *PPP1R15B* mutation in two siblings with young-onset diabetes, microcephaly and short stature. The mutation, located in the PP1 binding domain (8), disrupts PP1 binding and eIF2α dephosphorylation and reveals that β-cell dysfunction and apoptosis may be caused both by too little and by too much eIF2α phosphorylation.

RESEARCH DESIGN AND METHODS

Patients

We studied a consanguineous family from Algerian origin, with two siblings affected by young onset diabetes, associated with short stature, microcephaly and intellectual disability. The study was explained to the patients, their parents, tutors and other family members, who agreed to participate in the genetic study and signed informed consents. The study protocol was approved by the local ethics committee. Blood samples were obtained from the two affected siblings and two non-affected relatives (the paternal grand-mother and a paternal aunt) and DNA was extracted using standard procedures.

Exome sequencing and analysis

Exome sequencing was performed on the genomic platform of IntegraGen (Evry, France). Exons of genomic DNA of the index case (patient 1) were captured with in-solution enrichment methodology (SureSelect Human All Exon Kits version 2, Agilent) with the company's biotinylated oligonucleotide probe library (Human All Exon v2 50 Mb, Agilent). Genomic DNA was then sequenced on a sequencer as paired-end 75 bases (Illumina HISEQ 2000, Illumina, San Diego, USA). Image analysis and base calling were performed with Real

Time Analysis software version 1.14 with default parameters (Illumina). Bioinformatic analysis was performed by an in-house pipeline (IntegraGen) based on the Consensus Assessment of Sequence and Variation (CASAVA 1.8, Illumina) to perform alignment against human reference genome (GRCh37/hg19), variant calling and coverage analysis. The overall sequencing coverage over the whole exome was 88% and 79% for a 10X and 25X depth of coverage respectively, resulting in a mean sequencing depth of 64X per base. Exome variant analysis was then performed using an in-house python pipeline on genetic variation annotation results (M.D., unpublished). Variants were filtered consecutively based on their quality, their genotype (homozygous status), the predicted consequence on coding capacity (missense, nonsense, splice-site and coding insertion/deletion – inframe or frameshift), and for their rare status based on information available in in-house (control subjects, IntegraGen) and public databases (Exome Variant Server [EVS; ESP 6500], ExAC [release 0.3] and dbSNP v.138). Variants that were homozygous or had a minor allele frequency (MAF)>0.005 in any in-house or public database were excluded.

Variant confirmation and test for diabetes segregation in the family

Each rare variant identified as homozygous in patient 1 by exome sequencing was confirmed in patient 1 and further genotyped in patient 2, in two non-affected relatives (a paternal grand-mother and a paternal aunt) and in an unrelated healthy control subject. This was done by Sanger sequencing or by PCR-RFLP genotyping using specific amplification primers and restriction enzymes that differentiate the two alleles followed by agarose gel electrophoresis using standard techniques. Sequencing primers and PCR-RFLP primers/enzymes are available on request.

Sanger sequencing of *PPP1R15B* exons and regulatory regions

Sanger sequencing of *PPP1R15B* exons (coding, 5'UTR and 3'UTR regions) and flanking regions of a 680 bp of promoter region and a 800 bp intronic region that shows species conservation and contains unspliced human ESTs (UCSC Genome browser) was performed by Big Dye Terminator sequencing on PCR-amplified DNA using an Applied Biosystems 3730 DNA Sequencer (Foster City, CA, USA). PCR and sequencing primers are shown in Supplementary Table 1. Sequence interpretation was performed using the Genalys software (17).

Cell culture

Clonal rat INS-1E cells (a kind gift from Dr C Wollheim, Centre Médical Universitaire, Geneva, Switzerland) were cultured in RPMI medium as described (18). Male Wistar rats (Charles River Laboratories, Chatillon-sur-Chalaronne, France) were housed and handled following the rules of the Belgian Regulations for Animal Care. Rat tissues were collected and islets were handpicked under a stereomicroscope after isolation by collagenase digestion (19). β-cells were purified by autofluorescence-activated cell sorting of dispersed islet cells (FACS, FACSAria, BD Bioscience, Erembodegem, Belgium) and cultured as described (20). HEK293T cells were maintained in DMEM supplemented with 10% fetal bovine serum (FBS), 100 mU/ml penicillin, 100 mU/ml streptomycin and 2 mM L-glutamine.

Generation of the R658C mutant PPP1R15B expression plasmid

The R658C mutation was introduced in the PPP1R15BpEGFP_C1 plasmid (21) using Quick change II site directed mutagenesis kit (Agilent technologies, Santa Clara, California, USA) and the primers huPPP1R15B_R658C_1S: GTGGTGATGAGGAT**T**GCAAAGGACCATGG and huPPP1R15B_R658C_2AS: CCATGGTCCTTTGC**A**ATCCTCATCACCAC (bold letters

indicate the mutation site). This vector allows the expression of recombinant proteins fused to GFP at its N-terminus. After mutagenesis positive clones were sequenced (Seqlab, Göttingen, Germany) using the following primers to cover the entire gene: F1: CATGGTCCTGCTGGAGTTCGTG, F2: AGAGGAGGGGATCCACTG, F3: ACAGTGATGGAAATAGCGAG, F4: ATCTAGTGAGATACCTATGG, F5: TGAGACCCCTGAGCATAG, Rev: CACACCTCCCCCTGAAC. Plasmids containing the mutation, but no other change in the *PPP1R15B* gene, were introduced into one shot Top10 electro competent *E. coli* (Invitrogen, Gent, Belgium) by electroporation. The cells were recovered for 1h in SOC medium, plated on LB-agar containing 50 µg/ml kanamycin and incubated overnight at 37^{o}C. Selected colonies were grown overnight at 37°C on LB containing 50 µg/ml kanamycin. Plasmids were purified using the PureYield Plasmid midiprep kit (Promega, Leiden, the Netherlands) according to the manufacturer's instructions. The DNA concentration was measured using NanoDrop 3300 (Thermo Scientific, Gent, Belgium).

PPP1R15B over-expression and immunoprecipitation

HEK293T cells were transfected with pEGFP-plasmid without insert (empty vector) or expressing WT or mutant PPP1R15B, alone or combined with a mouse PP1A expression plasmid using PEI reagent. After 24h the cells were lysed as previously described (8).

Using 1 µl anti-GFP antibody bound to 15 µl protein-A sepharose resin, GFP-PPP1R15B was purified from equal amounts of cell lysate protein. The immunoprecipitates containing PPP1R15B were washed twice in lysis buffer before being resolved on a 10% SDS-PAGE gel and blotted onto PVDF membranes or used for dephosphorylation studies.

Dephosphorylation assay

PPP1R15B immunoprecipitates were resuspended in dephosphorylation buffer containing 50 mM Tris (pH 7), 100 mM NaCl, 0.1 mM EDTA, 0.1% Triton X-100, 1 mM DTT and 1 mM $MnCl_2$ and incubated with phosphorylated eIF2α for 5 to 60 minutes at 30°C. The supernatant was resolved on 15% phos-tagged SDS-PAGE gel and visualized using EZblue gel staining reagent (Sigma-Aldrich, Dorset, England).

RNA interference

Clonal and primary rat β-cells were transfected overnight with 30 nM control siRNA (Qiagen, Germantown, MD, USA) or siRNAs targeting rat PPP1R15B, DP5, PUMA or Bim using Lipofectamine RNAiMAX (Invitrogen) as described (22). The siRNAs utilized in the present study are listed in Supplementary Table 2.

Total RNA and mRNA extraction and real time PCR

Poly(A)$^+$ mRNA and total RNA were isolated and reverse transcribed as previously described (19;23). Real time PCR was performed using Rotor-Gene SyBR Green on a Rotor-Gene Q cycler (Qiagen) (23;24). Primers were used in a conventional PCR for preparing the standards. Gene expression was calculated as copies/µl (25). Expression levels were corrected for expression of the reference gene GAPDH. Primer sequences are provided in Supplementary Table 3.

Western blotting

Tissue and cell preparation was performed as previously described (26). Immunoblotting was done using antibodies against β-actin, P-eIF2α, eIF2α, BCL-2, BCL-XL, caspase 9, caspase 3, Cox IV (Cell Signaling, Leiden, the Netherlands), human α-tubulin (Sigma-Aldrich), human

ATF3, human PP1 (Santa Cruz, Heidelberg, Germany), cytochrome *c* (BD Biosciences) or GFP produced in rabbit. Protein detection was performed using DyLight conjugated secondary antibody or horseradish peroxidase-conjugated secondary antibodies and SuperSignal West Femto chemiluminescence revealing reagent (Thermo Scientific). Immunoreactive bands were detected with a ChemiDoc XRS+ system and with Image Lab software (BIO-RAD, Hercules, CA, USA). Protein levels were corrected for α-tubulin or β-actin.

Cell treatment and apoptosis assays

Free fatty acid (FFA) exposure was done in RPMI 1640 medium containing 0.75% FFA-free BSA (Roche, Mannheim, Germany) and 1% FBS. Oleate and palmitate (Sigma-Aldrich) were dissolved in 90% ethanol and diluted 1:100 to a final concentration of 0.5 mM (27;28). Cyclopiazonic acid (CPA) was used at 25 µM, tunicamycin at 5 µg/ml and brefeldin-A at 0.1 µg/ml. The PERK inhibitor GSK2606414 was used at 0.5 µM (29). Apoptotic cell death was detected and counted by fluorescence microscopy after Hoechst 33342 (5 µg/ml; Sigma-Aldrich) and propidium iodide (5 µg/ml) staining (28;30).

Glucose-stimulated insulin secretion

Insulin secretion was measured as described (22). Briefly, INS-1E cells were washed with modified Krebs-Ringer bicarbonate HEPES solution (KRB), incubated for 30 min with KRB without glucose, and insulin secretion was induced by 30 min incubation with KRB containing 1.67 or 16.7 mM glucose with or without 10 µM forskolin. Insulin was measured by ELISA (Mercodia, Uppsala, Sweden) in cell-free supernatants and acid-ethanol extracted cell lysates. Total protein was measured in cell lysates using the Protein Assay Dye Reagent (Biorad).

Cytochrome c release

Cells were harvested in PBS 48h after transfection. After centrifugation, cytosolic lysis buffer containing 0.8 μg/μl digitonin was added to the pellet. The cells were vortexed for 30s and centrifuged at 4°C at 20 000 Xg for 1 minute. The supernatant was separated as cytoplasmic fraction and the pellet was used as the mitochondrial fraction. Laemmli buffer was added and the samples were resolved on 12% SDS-PAGE.

Statistical analysis

Data are presented as means ± SE. Given the paired nature of the experimental design, comparisons between groups were made by two-sided Student's paired t test, with Bonferroni correction for multiple comparisons when needed. A p value <0.05 was considered statistically significant.

RESULTS

Description of a novel diabetes syndrome with young onset diabetes, short stature and microcephaly

We studied two siblings with young onset diabetes, intellectual disability, microcephaly and short stature who were born to non-diabetic first-cousin consanguineous parents (see Table 1 and Fig. 1 for the description of the patients). The index case (patient 1), a boy, was diagnosed with diabetes at age 15 years, with acute onset of polyuria and polydipsia. Fasting glucose was 13.4 mmol/l and HbA1c was 13.0% (119 mmol/mol). Type 1 diabetes specific autoantibodies (ICA, GAD, IA2) were negative. Fasting C-peptide was low but within normal range for normoglycemic subjects (Table 1), showing that at least some residual β-cell mass remained. He was treated by two daily insulin injections. Diabetes was initially well controlled with relatively low doses of insulin (~0.5 U/kg/day), but evolved to significant

glucose variability with severe hypoglycemia episodes and seizures. He had growth retardation (Fig. 1A), reaching adult height of 1.55 m, with normal growth hormone (GH peak at 41 ng /ml after ornithine stimulation test; N: >10) and IGF1 levels (291 μg/l; N:249-672). Thyroxine (18 pmol/l; N:10-23) and glucagon (116 ng/l; N:25-250) levels were normal. Blood cell count, electrolytes, creatinine, liver enzymes, bilirubin, cholesterol, triglycerides, lactate and pyruvate levels were normal. He had delayed puberty, with undescended right testis that was surgically corrected. No anomaly of the gonadal function was found, with normal levels of testosterone (9.54 nmol/l; N:9.0-26.0), LH (4.4 mU/ml; N:0.24-5.9) and FSH (6.5 mU/ml; N:1.9-11.6). He had microcephaly (adult cranial perimeter: 46 cm, -4.0 SD) and severe intellectual disability, with a quiet introverted character. At 15 years his mental level was comparable to that of a 5-6-year-old child. He answered questions using simple sentences but could not read or write. His vocabulary was limited to 200–300 words and he did not engage in conversation. He was able to perform tasks such as feeding, dressing and bathing but required full assistance in daily life. Magnetic resonance imaging showed rarefaction of the white matter (Fig. 1B), with non-specific slightly elevated level of protein in the cerebrospinal fluid (albumin and IgG). He had neurogenic deafness (hearing loss of 39%). He also had kyphoscoliosis, pectus excavatum and mild abnormalities of vertebral bodies (Fig. 1C and D), fine fingers and toes, oligodenty and dental hypoplasia, sparse hair and a high-pitched voice. Eye fundus was normal. Clinical and biochemical examination at 28 years showed that his diabetes was relatively well controlled (Table 1). Glucagon-stimulated C-peptide was detectable. Pubertal development was fully achieved (Tanner stage 5) with adult genitalia and complete epiphyseal closure on bone age X-ray. Biochemical measurements in serum showed low 25-hydroxyvitamin D (55 nmol/l; N:75-340), but normal levels of calcium, IGF-1 and thyroxine. Markers of phosphate metabolism were normal: PTH (19 pg/ml; N:10-55); serum phosphate (1.54 mmol/l; N:1.30-1.85); alkaline phosphatase (320 U/l; N:210-

830). Urinary calcium to creatinine ratio was also normal (0.33; N<0.7). His weight and BMI were low at 44.3 kg and 18.4 kg/m^2, respectively. Dual-energy X-ray absorptiometry showed normal body composition and bone mineral content. Overall, these results are in keeping with bone dysplasia without marked disturbance of calcium metabolism, with severe growth retardation unrelated to pituitary or thyroid dysfunction. Serum amylase, blood cell count, liver and kidney function and iron metabolism were normal. On ultrasound, liver and pancreas were normal, while the kidneys were small, with mild dilation of right calyces.

His sister (patient 2) had a similar clinical presentation, but she was not available for detailed evaluation. She had growth retardation, microcephaly, intellectual disability and diabetes presenting with an acute onset of hyperglycemia and ketosis at age 28 years. She was treated by insulin. She also had dental hypoplasia, an introverted character and high-pitched voice. She had menarche at the age of 14 years. At the last examination at 31 years, body weight was 30 kg, height 139 cm, BMI 15.5 kg/m^2 (Table 1). Blood cell count, electrolytes and kidney function parameters were normal. Early clinical history was unavailable for these patients, except for the information that they were born small for gestational age. The parents had normal fasting glucose (father: 5.1 mmol/l, mother: 4.3 mmol/l; N<5.6) and the mother was not known to have had gestational diabetes. They were unavailable for further clinical examination and genetic study.

Identification of a homozygous mutation in the *PPP1R15B* gene in the two diabetic siblings

Because of the familial context, we hypothesized that the syndrome was caused by an autosomal recessive mutation. To test this hypothesis, we performed exome sequencing on patient 1's genomic DNA and identified 18 rare homozygous autosomal variants after filtering (coding variants, minor allele frequency <0.005 and absence of subjects homozygous

for the rare variant in public and in-house databases; Supplementary Tables 4 and 5). We confirmed these variants in patient 1 and genotyped them in patient 2 and in two non-affected relatives (a grandmother and an aunt) by Sanger sequencing or PCR-RFLP genotyping. This reduced the number of variants to 6, for which both siblings, but not the unaffected relatives, were homozygous for the rare allele: *ADAMTSL4, FLG, KIF21B, PPP1R15B*, and *SLC45A3*, located on chromosome 1, and *UNC80,* located on chromosome 2 (Supplementary Tables 5 and ~~5~~6). Because of the relative similarities of this syndrome with Wolcott-Rallison syndrome (*EIF2AK3* mutations), the features of the *Ppp1r15b*$^{-/-}$ mouse (very small size at birth and early death) and its role in the ER stress response (31), *PPP1R15B* (Fig. 2A) appeared as the major candidate (Supplementary Table 6). None of the other genes showed obvious functional relevance to the syndrome (Supplementary Table 6). PPP1R15B is ubiquitously expressed (and well expressed in human islets and β-cells), consistent with the multi-system disease manifestations, while the other genes have a lower expression in islets, and their pattern of tissue expression does not specifically correspond to the syndrome (Supplementary Fig. 1, Supplementary Table 6). The R658 residue of *PPP1R15B* is highly conserved between organisms, including viruses (Fig. 2B) and the R658C mutation is predicted to be damaging by *in silico* prediction programs (Supplementary Table 6). It is located in the conserved C-terminal functional core of PPP1R15B that specifies interaction with PP1, the recruitment of the essential co-factor G-actin and substrate-specific dephosphorylation (21;32). In the co-crystal structure, PPP1R15B R658 inserts deep into a pocket on the surface of PP1 (34), giving rise to an ionic interaction with PP1 residue D71 that is conserved in other holophosphatases such as PP1-PPP1R10 (PNUTS) and PP1-PPP1R9B (spinophilin) (33). Collectively, these structural observations strongly support a critical role of R658 in PP1 binding and predict that mutation of this residue has deleterious effects on protein function.

To search for additional patients with *PPP1R15B* mutations, we performed Sanger sequencing of *PPP1R15B* exons, flanking regions, and main regulatory regions (Supplementary Table 1) in 50 patients with a similar clinical presentation, i.e. insulin-dependent diabetes and short stature and/or [mental retardation or microcephaly] and in 22 diabetic patients and their families compatible with monogenic diabetes and linkage to the *PPP1R15B* chromosome region (C.J., unpublished data), but we did not identify any homozygous or compound heterozygous *PPP1R15B* mutation in these patients.

The R658C mutation destabilizes the PPP1R15B-PP1 complex and impairs eIF2α dephosphorylation

To study the effect of the R658C mutation on PPP1R15B function we generated a plasmid encoding the fusion of wild-type (WT) or R658C mutated human PPP1R15B to EGFP. HEK293T cells were transfected with either plasmid or the empty pEGFP vector, alone or in combination with a plasmid expressing mouse PP1A. The PPP1R15B-PP1 complex was immunoprecipitated from cell lysates using anti-GFP antibody and analyzed for the presence of PP1 by Western blot. Less PP1 was recovered in complex with mutant PPP1R15B-EGFP compared to WT. This was true both when endogenous PP1 was examined (compare lanes 1 and 2, Fig. 3A) and when PP1A was overexpressed (compare lanes 5 and 6, Fig. 3A), demonstrating that the R658C mutation reduced the ability of PPP1R15B to bind PP1, as suggested by the structural studies.

Next we examined the dephosphorylation activity of the immunopurified PPP1R15B-PP1 holophosphatase complex. Complexes recovered by immunopurification of GFP-tagged WT PPP1R15B were more active at dephosphorylating eIF2α in vitro than complexes constituted of the R658C mutant (compare lanes 4 and 5 in Fig. 3B). These differences were rendered more conspicuous in a time course study: Complexes containing WT PPP1R15B substantially

dephosphorylated eIF2α protein by 45 minutes, whereas in dephosphorylation reactions carried out with R658C mutant PPP1R15B, substantial amounts of phosphorylated eIF2α remained even at the 60 minute time point (compare lanes 7 and 12, Fig. 3C). Thus, the missense mutation R658C negatively affects the stability of the PPP1R15B-PP1 complex and in turn its ability to dephosphorylate eIF2α.

PPP1R15B expression in β-cells

In clonal rat INS-1E β-cells PPP1R15B was induced by different synthetic ER stressors and the saturated FFA palmitate (Fig. 4A). This induction was prevented by a chemical inhibitor of PERK (Fig. 4B), suggesting that, different from other cell types (8), PPP1R15B expression in β-cells is controlled by the UPR.

PPP1R15B deficiency increases eIF2α phosphorylation in β-cells

Using RNA interference, PPP1R15B was knocked down in INS-1E cells, resulting in a 75% inhibition of mRNA expression (Fig. 4C). Consistent with its previously reported function of constitutive eIF2α phosphatase (8), basal eIF2α phosphorylation was increased in PPP1R15B-deficient INS-1E cells (Fig. 4D and E). PPP1R15B silencing did not further increase eIF2α phosphorylation induced by the synthetic ER stressor CPA or palmitate (Fig. 4D and E). P-eIF2α levels were higher in PPP1R15B-deficient cells exposed to the unsaturated FFA oleate that *per se* does not induce eIF2α phosphorylation (28;34). ATF3 protein was also induced in PPP1R15B-deficient cells under basal condition (Fig. 4F and G). Thus, PPP1R15B silencing increases eIF2α phosphorylation and induces downstream ATF3 protein expression.

PPP1R15B silencing decreases insulin content and glucose-stimulated insulin release

We next evaluated the effect of PPP1R15B deficiency on β-cell function. PPP1R15B knockdown decreased insulin content in INS-1E cells by 20% (Fig. 5A). In control siRNA transfected β-cells, high glucose exposure (16.7 mM) increased insulin secretion by 2.8-fold. PPP1R15B-deficient β-cells showed increased basal insulin secretion, and little or no response to high glucose (Fig. 5B). 16.7 mM glucose plus forskolin induced insulin secretion by 10-fold in control siRNA transfected cells, but only by 4-fold after PPP1R15B silencing ($p<0.05$).

PPP1R15B-deficient β-cells are sensitized to apoptosis through the pro-apoptotic BH3-only proteins DP5, PUMA and Bim

We examined the role of PPP1R15B in β-cell survival. PPP1R15B silencing in clonal (Fig. 6A and B) and primary rat β-cells (Fig. 6C) sensitized the cells to apoptosis under basal condition, and induced up to 20% more apoptosis following exposure to CPA or the FFAs oleate and palmitate (Fig. 6A-C).

To evaluate whether the intrinsic pathway of apoptosis was involved we measured mitochondrial cytochrome *c* release to the cytoplasm and cleavage of caspase-9 and -3. In PPP1R15B-deficient INS-1E cells, cytoplasmic cytochrome *c* levels were increased (Fig. 6D), and caspase-9 (Fig. 6E) and -3 (Fig. 6F) were cleaved, demonstrating activation of the intrinsic pathway of apoptosis.

We next examined which BCL-2 family members activate the intrinsic pathway of apoptosis. PPP1R15B deficiency induced mRNA expression of the pro-apoptotic proteins DP5 and PUMA (Fig. 6G and H), but it did not significantly affect expression of Bim-S protein (Fig. 6I). The expression of Bim-L and EL (Supplementary Fig. 2A-C) and the anti-apoptotic proteins BCL-2 and BCL-XL (Supplementary Fig. 2D-F) was not modified by PPP1R15B

deficiency. DP5, PUMA or Bim silencing partially protected PPP1R15B-silenced β-cells from apoptosis (Fig. 6J), showing that PPP1R15B deficiency induces apoptosis through the pro-apoptotic BH3-only proteins DP5, PUMA and Bim.

DISCUSSION

R658C is the first reported mutation in *PPP1R15B*, responsible for a novel diabetes syndrome with onset in youth/young adulthood. It affects a key amino acid in the conserved C-terminus region of the protein that makes contacts with PP1 that is conserved in other holophosphatase complexes (32;33). We presently show that the R658C mutation destabilizes the complex between PPP1R15B and PP1 and this in turn diminishes eIF2α dephosphorylation. Furthermore, we show that PPP1R15B silencing alters β-cell function, inducing higher basal insulin secretion and reducing high glucose responsiveness, which is compatible with a role of PPP1R15B in exocytosis (35). This is consistent with the observation of residual C-peptide in the index patient, his moderate insulin requirement and frequent hypoglycemic events. PPP1R15B silencing also sensitizes β-cells to apoptosis, both under basal and ER stress conditions, which was induced via the intrinsic pathway of apoptosis, as in the case of palmitate-induced eIF2α phosphorylation (36).

Of note, diabetes manifested relatively late in these patients (at ages 15 and 28 years). Considering the congenital nature of the defect, this suggests the role of compensatory mechanisms that maintain a sufficient β cell function for several years. The acute onset of diabetes suggests a threshold mechanism(s), by which this delicate balance is disrupted at some stage, as observed in autoimmune T1D and other forms of monogenic diabetes, leading to hyperglycemia (37).

The syndrome caused by the PPP1R15B-R658C mutation results in multisystem manifestations, affecting β-cells (diabetes), the nervous system (microcephaly, intellectual disability and hearing loss), bone (bone deformities) and general development. This phenotypic spectrum has interesting overlap with other mutations affecting the levels of ER stress or the response to it. Hence, β-cell dysfunction, bone abnormalities, microcephaly and intellectual disability are shared with Wolcott-Rallison syndrome caused by *EIF2AK3* mutations, that lead to higher levels of ER stress associated with less eIF2α phosphorylation (11;13;38), and in syndromes caused by mutations in the ER co-chaperone *DNAJC3* and in the immediate early response 3 interacting protein 1 (*IER3IP1*), that both lead to higher levels of ER stress with more eIF2α phosphorylation (16;39;40). These commonalities likely reflect the importance of balanced ER protein synthesis and folding to the function of secretory cells, with insulin-producing β-cells, collagen-producing bone cells and nerve cells especially vulnerable to imbalance. In Wolcott-Rallison syndrome (with decreased eIF2α phosphorylation) neonatal diabetes is due to β-cell loss and C-peptide is undetectable (13), while *DNAJC3, IER3IP1* and *PPP1R15B* mutations (with increased eIF2α phosphorylation) lead to permanent neonatal or young onset diabetes with residual C-peptide levels ((16;40) and this report). It is notable that mutations affecting the target of phosphorylated eIF2α, the guanine nucleotide exchange factor eIF2B, feature prominent neurodegenerative manifestations known as CACH (childhood ataxia with central nervous system hypomyelination)/VWM (leukoencephalopathy with vanishing white matter) syndrome (41), which are phenocopied by targeted activation of the eIF2α kinase PERK in the brain (42). Interestingly, severe forms of CACH/VWM also have multi-organ manifestations (41;43). The clinical variability of syndromes associated with dysregulated eIF2α phosphorylation likely results from the interplay of several factors including the extent of apoptosis and/or

secretory dysfunction resulting from specific genes mutations, the severity of the mutation and possibly environmental stresses.

The clinical features of *PPP1R15B* mutated patients described here and the phenotype of knockout mice that we described previously (31) suggest that PPP1R15B deficiency affects multiple cell types. The role of PPP1R15B in exocytosis and membrane traffic has been previously reported in human epithelial cells and erythroleukemia cells (35). Knockdown of PPP1R15B in breast cancer cells resulted in impaired cell cycle transition from G1 to S phase and apoptosis (44). These observations suggest that PPP1R15B regulates a variety of functions in different cell types. More studies are needed to explore this further.

Although we selected *PPP1R15B* as an obvious candidate gene, and found ample structural and functional experimental support for the impact of the mutation, we cannot formally exclude that one of the rare variants homozygous in the two affected siblings contributes to the syndrome. This hypothesis is unlikely based on the following reasons (Supplementary Table 6 and Supplementary Fig. 1): 1) None of the other genes appears directly functionally relevant to the clinical presentation; 2) The expression pattern of PPP1R15B, but not of the five other genes, is consistent with the multisystem presentation of the syndrome; 3) Mutations in *ADAMTSL4* cause ectopia lentis, while mutations in *FLG* cause atopic dermatitis and ichtyosis vulgaris; none of these diseases were present in the two affected siblings; 4) Human or mouse disease phenotypes of *KIF21B*, *SLC45A3*, and *UNC80* mutations have not been reported so far, and a cellular phenotype of chromosome instability has been reported in $Kif21b^{-/-}$ mice, which was not observed in our patients. In short, the characteristics of these five other genes show little relevance to the diabetes and neurological phenotype of our patients.

The present human genetic observations are in keeping with our earlier findings that excessive eIF2α phosphorylation is poorly tolerated by β-cells. Salubrinal, a chemical

inhibitor of eIF2α dephosphorylation, was identified in a large-scale chemical screening as a compound that protects from ER stress (45) and it was even suggested as a potential therapy to preserve β-cells in diabetes (46). In rodent and human β-cells, however, salubrinal actually exacerbates cell death through ER stress and downstream activation of the mitochondrial pathway of apoptosis (10;24). The present observations support the concept that dysregulation of eIF2α phosphorylation, either excessive (*PPP1R15B*, *DNAJC3* and *IER3IP1* mutations) or diminished (*EIF2AK3* mutations), is detrimental to β-cells, neurons and bone and suggest that other proteins involved in the regulation of protein translation may lead to similar diabetes syndromes.

ACKNOWLEDGEMENTS

We are very grateful to the patients and their family for their participation in the study. This work was supported by the European Union (project BetaBat in the Framework Programme 7), the Actions de Recherche Concertée de la Communauté Française (ARC) and Fonds National de la Recherche Scientifique (FNRS), Belgium, and by grants from the Agence Nationale pour la Recherche (ANR-09-GENO-021), the European Foundation for the Study of Diabetes (EFSD)/Juvenile Diabetes Research Foundation (JDRF)/NOVO Nordisk, the Assistance Publique-Hôpitaux de Paris (AP-HP, Programme Hospitalier de Recherche Clinique DIAGENE), the GIS-Maladies Rares and the Wellcome Trust (084812/Z/08/Z). ATH is a Welcome Trust and NIHR senior investigator and DR is a Wellcome Trust Principal Research Fellow. We thank Christophe Caloustian and Sylvana Pavek from the CNG for expert technical assistance. We are grateful to the Flow Cytometry Facility of the Erasmus Campus of the ULB and Christine Dubois for the cell sorting. We thank Michael Pangerl, Anyishai Musuaya, Nathalie Pachera, Stephanie Mertens and Isabelle Millard at the ULB Center for Diabetes Research for excellent technical support. BA was supported by an EMBO Short Term Fellowship and an FNRS-FRIA fellowship, MD by a doctoral fellowship from the Ministère de l'Education Nationale, de l'Enseignement Supérieur et de la Recherche, France. MIE is a scientific collaborator of the FNRS. We thank Annabelle Chaussenot from the School of Medicine, Nice Sophia-Antipolis University for contributing some patients for this study and for interesting discussions. We thank Dr Belkacem Bioud, University Hospital of Setif, Algeria and Dr Hadda Baaziz, University Hospital of Batna, Algeria, for their collaboration.

AUTHOR CONTRIBUTIONS

B.A., M.N., A.P., D.R., D.L.E., M.C and C.J contributed to the study design; M.D., S.R., A.P., V.S., C.D. and C.J. performed the genetic experiments, analyzed and interpreted the genetic data; B.A., M.I.-E., M.L., D.A.C., H.P.H, D.R., D.L.E and M.C. performed the functional experiments, analyzed and interpreted the functional data; M.N. and N.B. identified the index patient and family and characterized these patients; M.N., N.B., and A.T.H. contributed patients; B.A., M.N., A.P., D.R., M.C. and C.J wrote the manuscript. All co-authors read and approved the manuscript. C.J. is the guarantor of this work and, as such, had full access to all the data in the study and takes responsibility for the integrity of the data and the accuracy of the data analysis.

COMPETING INTERESTS

None

REFERENCES

1. Eizirik DL, Cardozo AK, Cnop M. The role for endoplasmic reticulum stress in diabetes mellitus. Endocr Rev 2008;29:42-61
2. Cnop M, Foufelle F, Velloso LA. Endoplasmic reticulum stress, obesity and diabetes. Trends Mol Med 2012;18:59-68
3. Marhfour I, Lopez XM, Lefkaditis D, Salmon I, Allagnat F, Richardson SJ, Morgan NG, Eizirik DL. Expression of endoplasmic reticulum stress markers in the islets of patients with type 1 diabetes. Diabetologia 2012;55:2417-2420
4. Laybutt DR, Hawkins YC, Lock J, Lebet J, Sharma A, Bonner-Weir S, Weir GC. Influence of diabetes on the loss of beta cell differentiation after islet transplantation in rats. Diabetologia 2007;50:2117-2125

5. Marchetti P, Bugliani M, Lupi R, Marselli L, Masini M, Boggi U, Filipponi F, Weir GC, Eizirik DL, Cnop M. The endoplasmic reticulum in pancreatic beta cells of type 2 diabetes patients. Diabetologia 2007;50:2486-2494
6. Hartman MG, Lu D, Kim ML, Kociba GJ, Shukri T, Buteau J, Wang X, Frankel WL, Guttridge D, Prentki M, Grey ST, Ron D, Hai T. Role for activating transcription factor 3 in stress-induced beta-cell apoptosis. Mol Cell Biol 2004;24:5721-5732
7. Ron D, Walter P. Signal integration in the endoplasmic reticulum unfolded protein response. Nat Rev Mol Cell Biol 2007;8:519-529
8. Jousse C, Oyadomari S, Novoa I, Lu P, Zhang Y, Harding HP, Ron D. Inhibition of a constitutive translation initiation factor 2α phosphatase, CReP, promotes survival of stressed cells. J Cell Biol 2003;163:767-775
9. Novoa I, Zeng H, Harding HP, Ron D. Feedback inhibition of the unfolded protein response by GADD34-mediated dephosphorylation of eIF2alpha. J Cell Biol 2001;153:1011-1022
10. Cnop M, Ladriere L, Hekerman P, Ortis F, Cardozo AK, Dogusan Z, Flamez D, Boyce M, Yuan J, Eizirik DL. Selective inhibition of eukaryotic translation initiation factor 2 alpha dephosphorylation potentiates fatty acid-induced endoplasmic reticulum stress and causes pancreatic beta-cell dysfunction and apoptosis. J Biol Chem 2007;282:3989-3997
11. Delepine M, Nicolino M, Barrett T, Golamaully M, Lathrop GM, Julier C. EIF2AK3, encoding translation initiation factor 2-alpha kinase 3, is mutated in patients with Wolcott-Rallison syndrome. Nat Genet 2000;25:406-409
12. Scheuner D, Song B, McEwen E, Liu C, Laybutt R, Gillespie P, Saunders T, Bonner-Weir S, Kaufman RJ. Translational control is required for the unfolded protein response and in vivo glucose homeostasis. Mol Cell 2001;7:1165-1176
13. Julier C, Nicolino M. Wolcott-Rallison syndrome. Orphanet J Rare Dis 2010;5:29

14. Harding HP, Zeng H, Zhang Y, Jungries R, Chung P, Plesken H, Sabatini DD, Ron D. Diabetes mellitus and exocrine pancreatic dysfunction in perk-/- mice reveals a role for translational control in secretory cell survival. Mol Cell 2001;7:1153-1163
15. Stoy J, Edghill EL, Flanagan SE, Ye H, Paz VP, Pluzhnikov A, Below JE, Hayes MG, Cox NJ, Lipkind GM, Lipton RB, Greeley SA, Patch AM, Ellard S, Steiner DF, Hattersley AT, Philipson LH, Bell GI. Insulin gene mutations as a cause of permanent neonatal diabetes. Proc Natl Acad Sci U S A 2007;104:15040-15044
16. Synofzik M, Haack TB, Kopajtich R, Gorza M, Rapaport D, Greiner M, Schonfeld C, Freiberg C, Schorr S, Holl RW, Gonzalez MA, Fritsche A, Fallier-Becker P, Zimmermann R, Strom TM, Meitinger T, Zuchner S, Schule R, Schols L, Prokisch H. Absence of BiP co-chaperone DNAJC3 causes diabetes mellitus and multisystemic neurodegeneration. Am J Hum Genet 2014;95:689-697
17. Takahashi M, Matsuda F, Margetic N, Lathrop M. Automated identification of single nucleotide polymorphisms from sequencing data. J Bioinform Comput Biol 2003;1:253-265
18. Ortis F, Cardozo AK, Crispim D, Storling J, Mandrup-Poulsen T, Eizirik DL. Cytokine-induced proapoptotic gene expression in insulin-producing cells is related to rapid, sustained, and nonoscillatory nuclear factor-κB activation. Mol Endocrinol 2006;20:1867-1879
19. Rasschaert J, Ladriere L, Urbain M, Dogusan Z, Katabua B, Sato S, Akira S, Gysemans C, Mathieu C, Eizirik DL. Toll-like receptor 3 and STAT-1 contribute to double-stranded RNA+ interferon-γ-induced apoptosis in primary pancreatic β-cells. J Biol Chem 2005;280:33984-33991

20. Marroqui L, Masini M, Merino B, Grieco FA, Millard I, Dubois C, Quesada I, Marchetti P, Cnop M, Eizirik DL. Pancreatic α cells are resistant to metabolic stress-induced apoptosis in type 2 diabetes. EBioMedicine 2015

21. Chambers JE, Dalton LE, Clarke HJ, Malzer E, Dominicus CS, Patel V, Moorhead G, Ron D, Marciniak SJ. Actin dynamics tune the integrated stress response by regulating eukaryotic initiation factor 2alpha dephosphorylation. Elife 2015;4:

22. Cnop M, Igoillo-Esteve M, Rai M, Begu A, Serroukh Y, Depondt C, Musuaya AE, Marhfour I, Ladriere L, Moles L, X, Lefkaditis D, Moore F, Brion JP, Cooper JM, Schapira AH, Clark A, Koeppen AH, Marchetti P, Pandolfo M, Eizirik DL, Fery F. Central role and mechanisms of β-cell dysfunction and death in friedreich ataxia-associated diabetes. Ann Neurol 2012;72:971-982

23. Kharroubi I, Ladriere L, Cardozo AK, Dogusan Z, Cnop M, Eizirik DL. Free fatty acids and cytokines induce pancreatic β-cell apoptosis by different mechanisms: role of nuclear factor-κB and endoplasmic reticulum stress. Endocrinology 2004;145:5087-5096

24. Ladriere L, Igoillo-Esteve M, Cunha DA, Brion JP, Bugliani M, Marchetti P, Eizirik DL, Cnop M. Enhanced signaling downstream of ribonucleic Acid-activated protein kinase-like endoplasmic reticulum kinase potentiates lipotoxic endoplasmic reticulum stress in human islets. J Clin Endocrinol Metab 2010;95:1442-1449

25. Overbergh L, Valckx D, Waer M, Mathieu C. Quantification of murine cytokine mRNAs using real time quantitative reverse transcriptase PCR. Cytokine 1999;11:305-312

26. Moore F, Colli ML, Cnop M, Esteve MI, Cardozo AK, Cunha DA, Bugliani M, Marchetti P, Eizirik DL. PTPN2, a candidate gene for type 1 diabetes, modulates interferon-γ-induced pancreatic β-cell apoptosis. Diabetes 2009;58:1283-1291

27. Cnop M, Hannaert JC, Hoorens A, Eizirik DL, Pipeleers DG. Inverse relationship between cytotoxicity of free fatty acids in pancreatic islet cells and cellular triglyceride accumulation. Diabetes 2001;50:1771-1777

28. Cunha DA, Hekerman P, Ladriere L, Bazarra-Castro A, Ortis F, Wakeham MC, Moore F, Rasschaert J, Cardozo AK, Bellomo E, Overbergh L, Mathieu C, Lupi R, Hai T, Herchuelz A, Marchetti P, Rutter GA, Eizirik DL, Cnop M. Initiation and execution of lipotoxic ER stress in pancreatic β-cells. J Cell Sci 2008;121:2308-2318

29. Harding HP, Zyryanova AF, Ron D. Uncoupling proteostasis and development in vitro with a small molecule inhibitor of the pancreatic endoplasmic reticulum kinase, PERK. J Biol Chem 2012;287:44338-44344

30. Igoillo-Esteve M, Marselli L, Cunha DA, Ladriere L, Ortis F, Grieco FA, Dotta F, Weir GC, Marchetti P, Eizirik DL, Cnop M. Palmitate induces a pro-inflammatory response in human pancreatic islets that mimics CCL2 expression by beta cells in type 2 diabetes. Diabetologia 2010;53:1395-1405

31. Harding HP, Zhang Y, Scheuner D, Chen JJ, Kaufman RJ, Ron D. Ppp1r15 gene knockout reveals an essential role for translation initiation factor 2 alpha (eIF2alpha) dephosphorylation in mammalian development. Proc Natl Acad Sci U S A 2009;106:1832-1837

32. Chen R, Rato C, Yan Y, Crespillo-Casado A, Clarke HJ, Harding HP, Marciniak SJ, Read RJ, Ron D. G-actin provides substrate-specificity to eukaryotic initiation factor 2alpha holophosphatases. Elife 2015;4:

33. Choy MS, Hieke M, Kumar GS, Lewis GR, Gonzalez-DeWhitt KR, Kessler RP, Stein BJ, Hessenberger M, Nairn AC, Peti W, Page R. Understanding the antagonism of retinoblastoma protein dephosphorylation by PNUTS provides insights into the PP1 regulatory code. Proc Natl Acad Sci U S A 2014;111:4097-4102

34. Karaskov E, Scott C, Zhang L, Teodoro T, Ravazzola M, Volchuk A. Chronic palmitate but not oleate exposure induces endoplasmic reticulum stress, which may contribute to INS-1 pancreatic β-cell apoptosis. Endocrinology 2006;147:3398-3407

35. Kloft N, Neukirch C, von HG, Bobkiewicz W, Weis S, Boller K, Husmann M. A subunit of eukaryotic translation initiation factor 2alpha-phosphatase (CreP/PPP1R15B) regulates membrane traffic. J Biol Chem 2012;287:35299-35317

36. Cunha DA, Igoillo-Esteve M, Gurzov EN, Germano CM, Naamane N, Marhfour I, Fukaya M, Vanderwinden JM, Gysemans C, Mathieu C, Marselli L, Marchetti P, Harding HP, Ron D, Eizirik DL, Cnop M. Death protein 5 and p53-upregulated modulator of apoptosis mediate the endoplasmic reticulum stress-mitochondrial dialog triggering lipotoxic rodent and human β-cell apoptosis. Diabetes 2012;61:2763-2775

37. Eizirik DL, Sandler S, Palmer JP. Repair of pancreatic beta-cells. A relevant phenomenon in early IDDM? Diabetes 1993;42:1383-1391

38. de Wit MC, de Coo IF, Julier C, Delepine M, Lequin MH, van dL, I, Sibbles BJ, Bruining GJ, Mancini GM. Microcephaly and simplified gyral pattern of the brain associated with early onset insulin-dependent diabetes mellitus. Neurogenetics 2006;7:259-263

39. Poulton CJ, Schot R, Kia SK, Jones M, Verheijen FW, Venselaar H, de Wit MC, de GE, Bertoli-Avella AM, Mancini GM. Microcephaly with simplified gyration, epilepsy, and infantile diabetes linked to inappropriate apoptosis of neural progenitors. Am J Hum Genet 2011;89:265-276

40. Shalev SA, Tenenbaum-Rakover Y, Horovitz Y, Paz VP, Ye H, Carmody D, Highland HM, Boerwinkle E, Hanis CL, Muzny DM, Gibbs RA, Bell GI, Philipson LH, Greeley SA. Microcephaly, epilepsy, and neonatal diabetes due to compound heterozygous

mutations in IER3IP1: insights into the natural history of a rare disorder. Pediatr Diabetes 2014;15:252-256

41. Fogli A, Boespflug-Tanguy O. The large spectrum of eIF2B-related diseases. Biochem Soc Trans 2006;34:22-29
42. Lin Y, Pang X, Huang G, Jamison S, Fang J, Harding HP, Ron D, Lin W. Impaired eukaryotic translation initiation factor 2B activity specifically in oligodendrocytes reproduces the pathology of vanishing white matter disease in mice. J Neurosci 2014;34:12182-12191
43. van der Knaap MS, van Berkel CG, Herms J, van CR, Baethmann M, Naidu S, Boltshauser E, Willemsen MA, Plecko B, Hoffmann GF, Proud CG, Scheper GC, Pronk JC. eIF2B-related disorders: antenatal onset and involvement of multiple organs. Am J Hum Genet 2003;73:1199-1207
44. Shahmoradgoli M, Riazalhosseini Y, Haag D, Becker N, Hovestadt V, Heck S, Sinn HP, Schneeweiss A, Mannherz O, Sahin O, Lichter P. Protein phosphatase 1, regulatory subunit 15B is a survival factor for ERalpha-positive breast cancer. Int J Cancer 2013;132:2714-2719
45. Boyce M, Bryant KF, Jousse C, Long K, Harding HP, Scheuner D, Kaufman RJ, Ma D, Coen DM, Ron D, Yuan J. A selective inhibitor of eIF2alpha dephosphorylation protects cells from ER stress. Science 2005;307:935-939
46. Wiseman RL, Balch WE. A new pharmacology--drugging stressed folding pathways. Trends Mol Med 2005;11:347-350

Table 1: Clinical and biochemical characteristics of the two patients

	Patient 1		Patient 2
Gender	Male		Female
Age at diabetes onset, years	15		28
Age at follow-up examination, years	15*	28	31
Anthropometry			
Height, cm (SD)	146 (-3.5)	155 (-3.2)	139 (-4.2)
Weight, kg (SD)	31.4 (-3.2)	44.3 (-3.5)	30 (-4.0)
BMI, kg/m2 (SD)	14.7 (-2.7)	18.4 (-1.7)	15.5 (-2.5)
Microcephaly	Yes	Yes	Yes
Cranial perimeter, cm (SD)	46 (-4.0)	46 (-4.0)	NA
Glucose metabolism			
HbA_{1c}, % [N: 4.0-6.0]	13.0	7.8	NA
C-peptide secretion evaluation			
Glycemia, fasting, mmol/l [N: <5.6]	3.96	11.4	NA
C-peptide, fasting, nmol/l [N: 0.25-1.28]	0.56	NA	NA
C-peptide, glucagon-stimulated [N: >0.6]	NA	0.89	NA
Therapy			
Insulin therapy duration, years	0	13	3
Insulin dose, U/kg/day	0	0.5	0.7

Notes: * at diabetes onset. BMI = Body mass index; NA = not available. N: Normal reference values. Standard deviations (SD) are based on French normative values.

FIGURE LEGENDS

Figure 1: Imaging of brain and skeleton of patient 1. A. Growth chart, showing growth retardation. B. Coronal T2-weighted brain magnetic resonance imaging at age 15 years, showing a moderate white matter rarefaction characterized by increased sulcal size and moderate enlargement of ventricular system. C, D. Skeletal radiographies at age 28 years, showing kyphoscoliosis with tall vertebral bodies and hyperlordosis.

Figure 2: Identification of a homozygous PPP1R15B-R658C mutation in two diabetic siblings and consequences of the mutation on the protein. (A) Sanger sequencing of a control subject and the two diabetic siblings (filled symbols), presenting the homozygous mutation and its consequence on the cDNA and protein. (B) PPP1R15B protein sequence, showing the alignment of a highly conserved 62 amino-acid segment (hatched) located within the C-terminal functional core region (gray). Representative sequences aligned are PPP1R15B from human (PR15B_HUMAN, Q5SWA1) and mouse (PR15B_MOUSE, Q8BFW3), PPP1R15A from human (PR15A_HUMAN, O75807), mouse (PR15A_MOUSE, P17564) and drosophila (PR15A_DROME, Q9W1E4), and homologous proteins from a variety of viruses: African Swine fever virus (VF71_ASFB7, Q65212), Amsacta moorei entomopoxvirus L (NP_064975), Glossina pallidipes salivary gland hypertrophy virus (YP_001687092), Choristoneura occidentalis granulovirus (YP_654457) and Trichoplusia niascovirus 2c (YP_803309). The mutated Arginine (R) at position 658 is part of the functional RVxF-ΦΦ-R motif (boxed and underlined on human PPP1R15B), that has been recognized in PP1 interacting proteins (33). Residues shown in red are fully conserved in selected species; residues that are the most critical for establishing contact with PP1 according to Chen et al. (32) are indicated by stars.

Figure 3: **The R658C mutation destabilizes the PPP1R15B-PP1 complex and diminishes its phosphatase activity.** HEK293T cells were transfected with an empty vector (GFP) or a GFP-tagged wild-type (WT) or R658C mutated (Mut PPP1R15B) human PPP1R15B, alone or in combination with a mouse PP1A expression plasmid**.** PPP1R15B-PP1 complexes were immunoprecipitated from lysed cells with anti-GFP antibody. (A) The recovery of PP1 in complex with PPP1R15B was examined by Western blotting using anti-PP1 antibody. Immunoprecipitated protein is shown on the left (IP) and the eluent is shown on the right (input). (B) The holophosphatase activity was studied in an eIF2α dephosphorylation assay, incubating the indicated PPP1R15B-PP1 complexes purified from cells with in vitro phosphorylated P-eIF2α protein for 30 min and resolving the phosphorylated and non-phosphorylated eIF2α on PhosTag gels. (C) A time course of eIF2α dephosphorylation by WT and Mut PPP1R15B-PP1A complexes recovered by immunopurification from transfected HEK293T cells. Unphosphorylated eIF2α was loaded onto lane 1 as a reference. The blots are representative of 3 or more independent experiments with similar outcomes.

Figure 4: **PPP1R15B is induced by ER stress in β-cells in a PERK-dependent manner and PPP1R15B silencing induces eIF2α phosphorylation and ATF3 in β-cells.** (A) INS-1E cells were exposed to the chemical ER stressors CPA, tunicamycin (TU) or brefeldin A (BR), or the FFAs oleate (OL) or palmitate (PAL) for 24h (n=5-6). (B) INS-1E cells were exposed or not (CT) to CPA in the presence or absence of the PERK inhibitor GSK2606414 (PERKi). PPP1R15B mRNA expression was examined by real time PCR and normalized to the reference gene GAPDH. (C) INS-1E cells were transfected with control siRNA (siCT) or two different siRNAs targeting PPP1R15B (P1R15B1 and P1R15B2). 48h after transfection the cells were treated for 16h with CPA, oleate (OL) or palmitate (PAL). PPP1R15B mRNA expression was examined by real time PCR and normalized to the reference gene GAPDH

(n=4). eIF2α phosphorylation (P-eIF2α) (D, E) and ATF3 (F, G) expression were examined by Western blot. (D) and (F) are representative images of n=4. (E) and (G) represent densitometric quantifications of (D) and (F) respectively. P-eIF2α was corrected for total eIF2α. ATF3 expression was corrected for α-tubulin and expressed as fold of CT. Data are presented as means ± SE. *treated vs control, §DMSO vs PERKi, #siP1R15B vs siCT by two-sided Student's paired t test, */§/#p<0.05, **/##p<0.01, ***/###p<0.001

Figure 5: **Glucose-stimulated insulin secretion is blunted by PPP1R15B deficiency in β-cells.** INS-1E cells were transfected with control siRNA (siCT) or two siRNAs targeting PPP1R15B (siP1R15B1 and siP1R15B2). 48h after transfection insulin secretion was induced by 1.67 or 16.7 mM glucose or 16.7 mM glucose + 10 μM forskolin (16.7+FK). (A) Cellular insulin content corrected for total protein. (B) Insulin release as percent of insulin content (n=5). *vs 1.67 mM glucose, **p<0.01, ***p<0.001. #siP1R15B vs siCT, #p<0.05, ##p<0.01 as indicated by the bars.

Figure 6: **PPP1R15B deficiency sensitizes β-cells to FFA- and ER stress-induced apoptosis and activates the intrinsic pathway of apoptosis via DP5, PUMA and Bim-S.** INS-1E (A, B) or primary rat β-cells (C) were transfected with a control siRNA (siCT) or two different siRNAs targeting PPP1R15B (siP1R15B1 and siP1R15B2). 24h after transfection the cells were exposed or not (CT) to CPA, oleate (OL) or palmitate (PAL) for 16 (A, B) or 24h (C) (n=4-5). (D) Mitochondrial cytochrome *c* release was detected by Western blot in the cytoplasmic fraction 48h after PPP1R15B knockdown. The right lane shows a non-cytoplasmic fraction that includes mitochondria. Cox IV was used as mitochondrial control and β-actin as cytoplasmic control. Activation of caspase-9 (Casp9) (E) and -3 (Casp3) (F) was detected by Western blot 48h after PPP1R15B knockdown. β-actin and α-tubulin were

used as loading controls. D, E and F are representative blots of 4-5 experiments. The densitometry data were normalized to the highest value. DP5 (G) and PUMA (H) mRNA expression was measured by real time PCR and corrected for the reference gene GAPDH (n=4). Bim-S levels were measured by Western blot (Supplementary Fig. 2), corrected for α-tubulin and expressed as fold of siCT (I) (n=5). (J) PPP1R15B was silenced alone or in combination with DP5, PUMA or Bim and apoptosis was examined by Hoechst33342/propidium iodide staining (n=3-4). *treated vs control, *$p<0.05$, **$p<0.01$, ***$p<0.001$. #siP1R15B vs siCT, #$p<0.05$, ##$p<0.01$, ###$p<0.001$, §single vs double knockdown, §$p<0.05$.

Figure 1

A

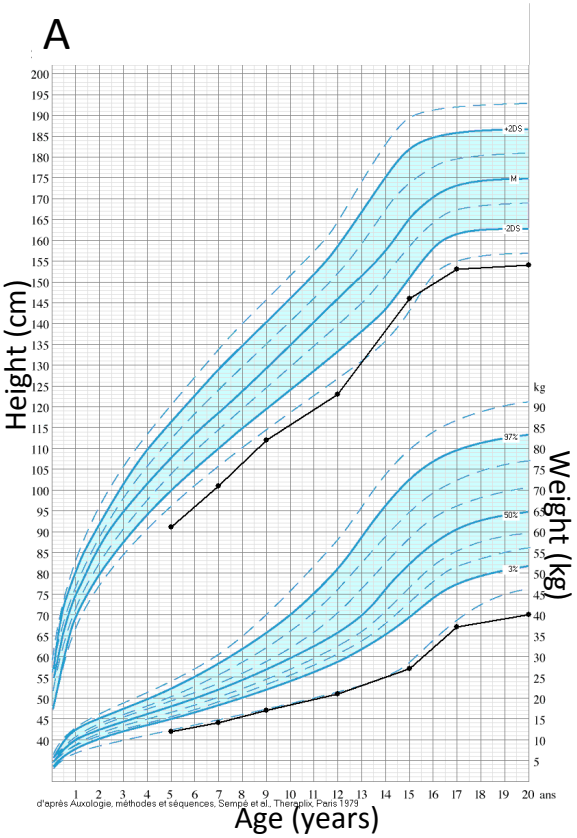

B

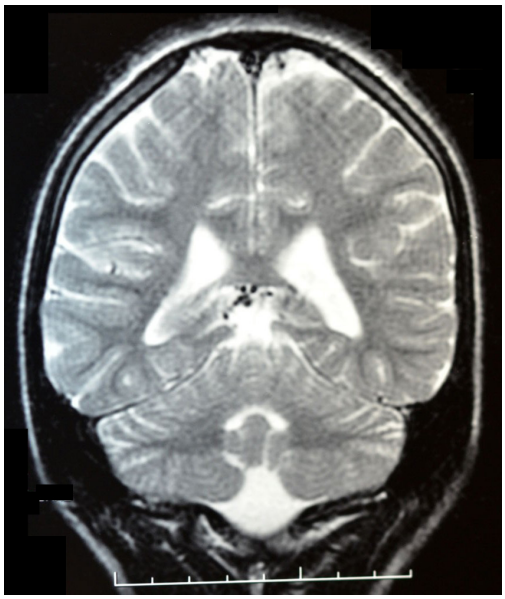

C

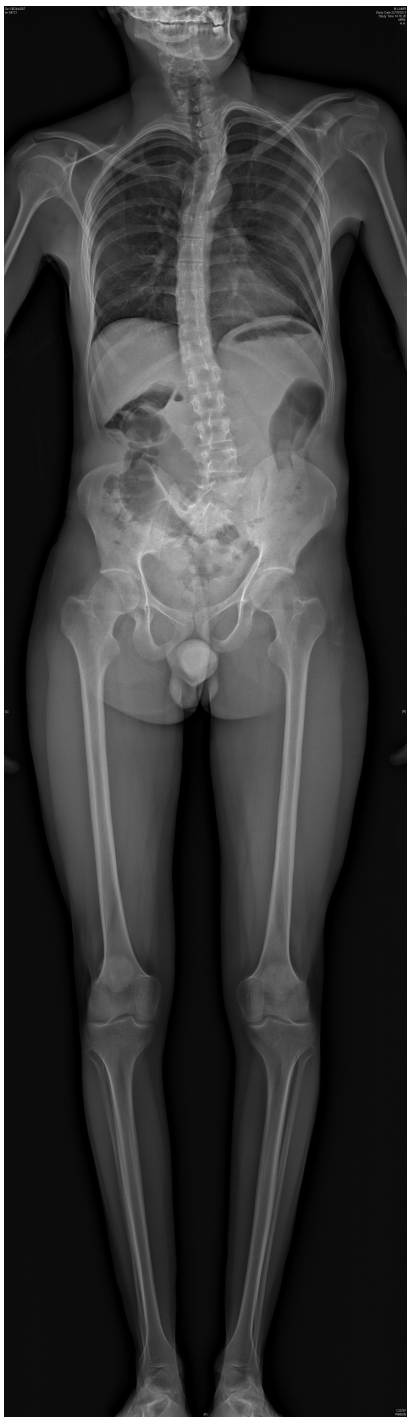

D

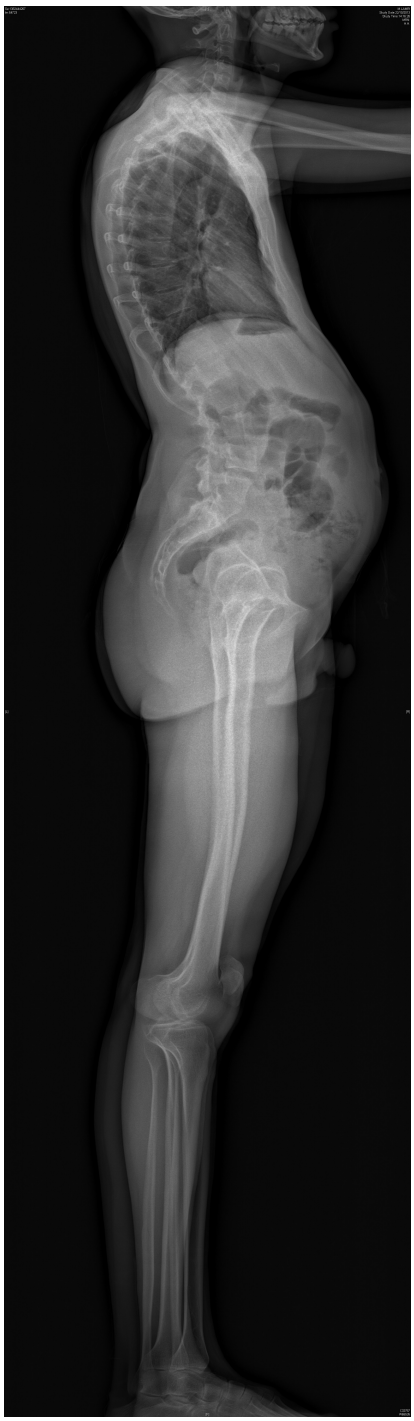

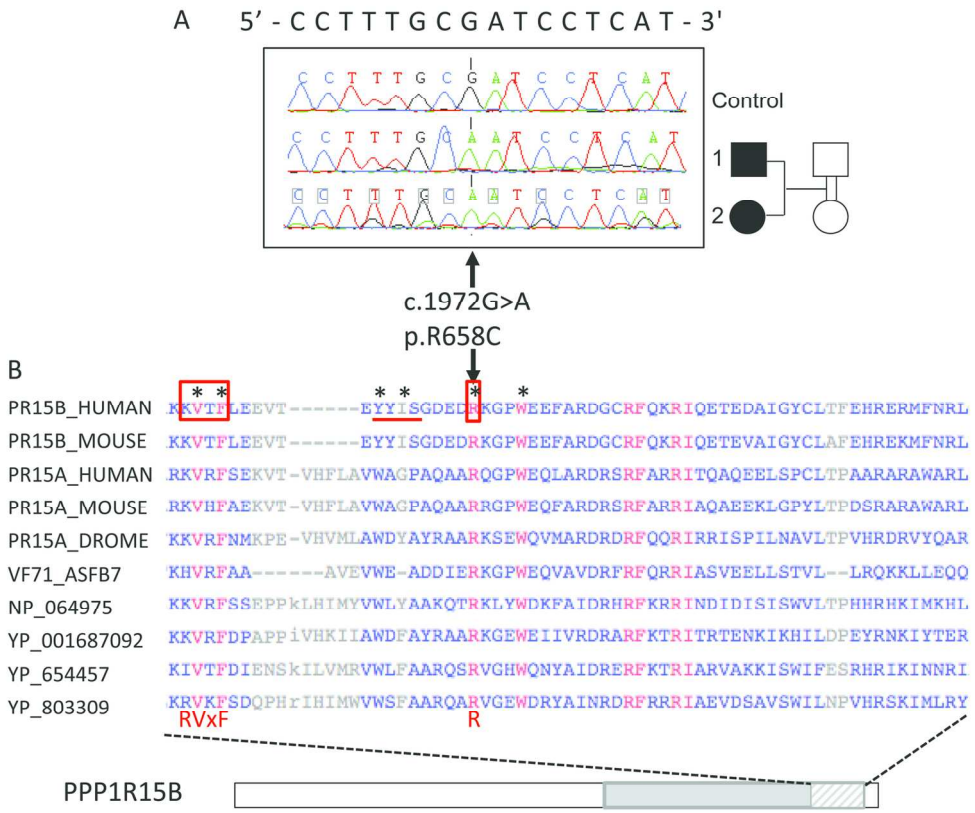

Figure 2
145x118mm (300 x 300 DPI)

Figure 3

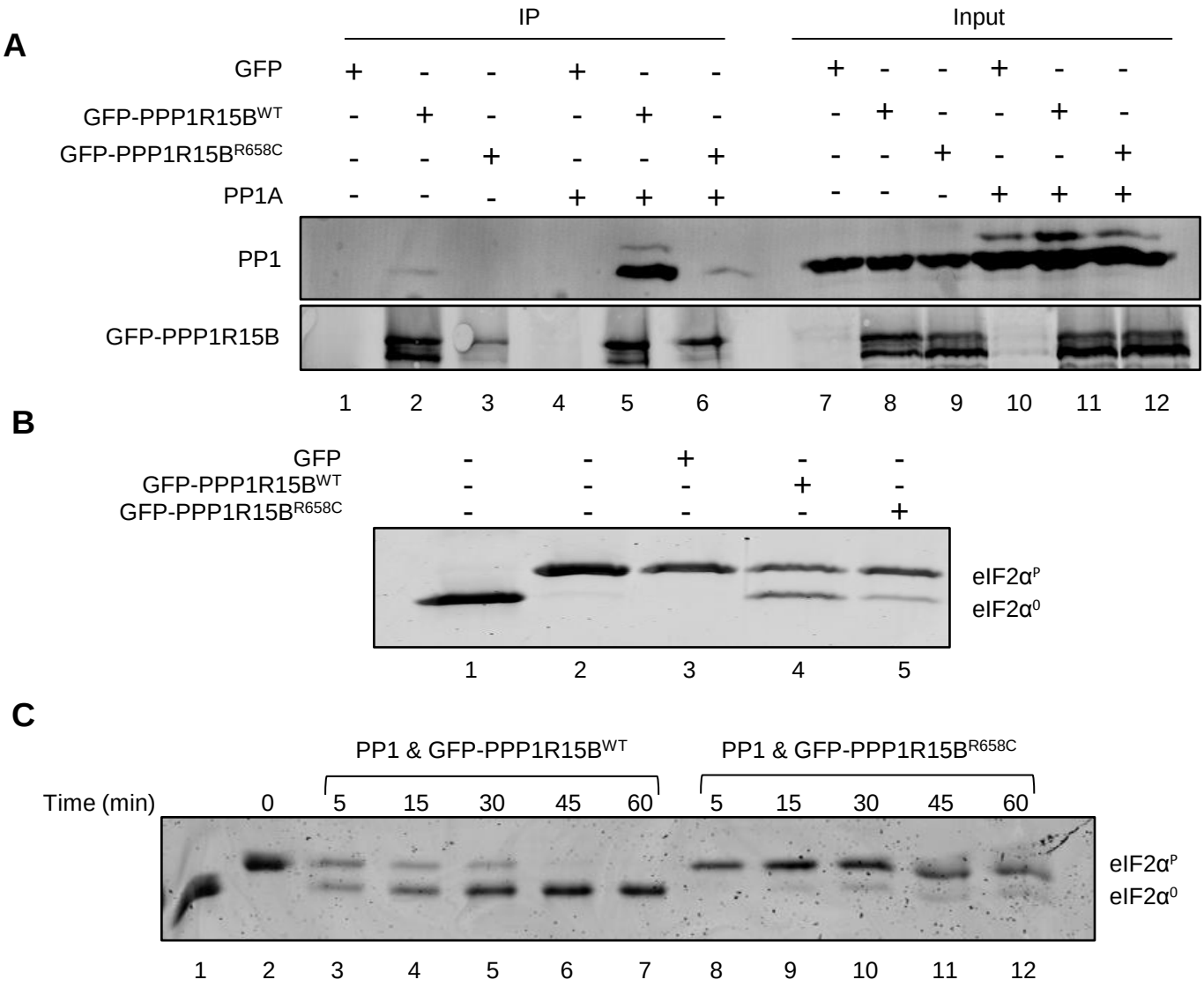
A
IP
Input
GFP
GFP-PPP1R15B^WT
GFP-PPP1R15B^R658C
PP1A
PP1
GFP-PPP1R15B
1 2 3 4 5 6 7 8 9 10 11 12
B
GFP
GFP-PPP1R15B^WT
GFP-PPP1R15B^R658C
eIF2α^P
eIF2α^0
1 2 3 4 5
C
PP1 & GFP-PPP1R15B^WT
PP1 & GFP-PPP1R15B^R658C
Time (min)
0 5 15 30 45 60 5 15 30 45 60
eIF2α^P
eIF2α^0
1 2 3 4 5 6 7 8 9 10 11 12

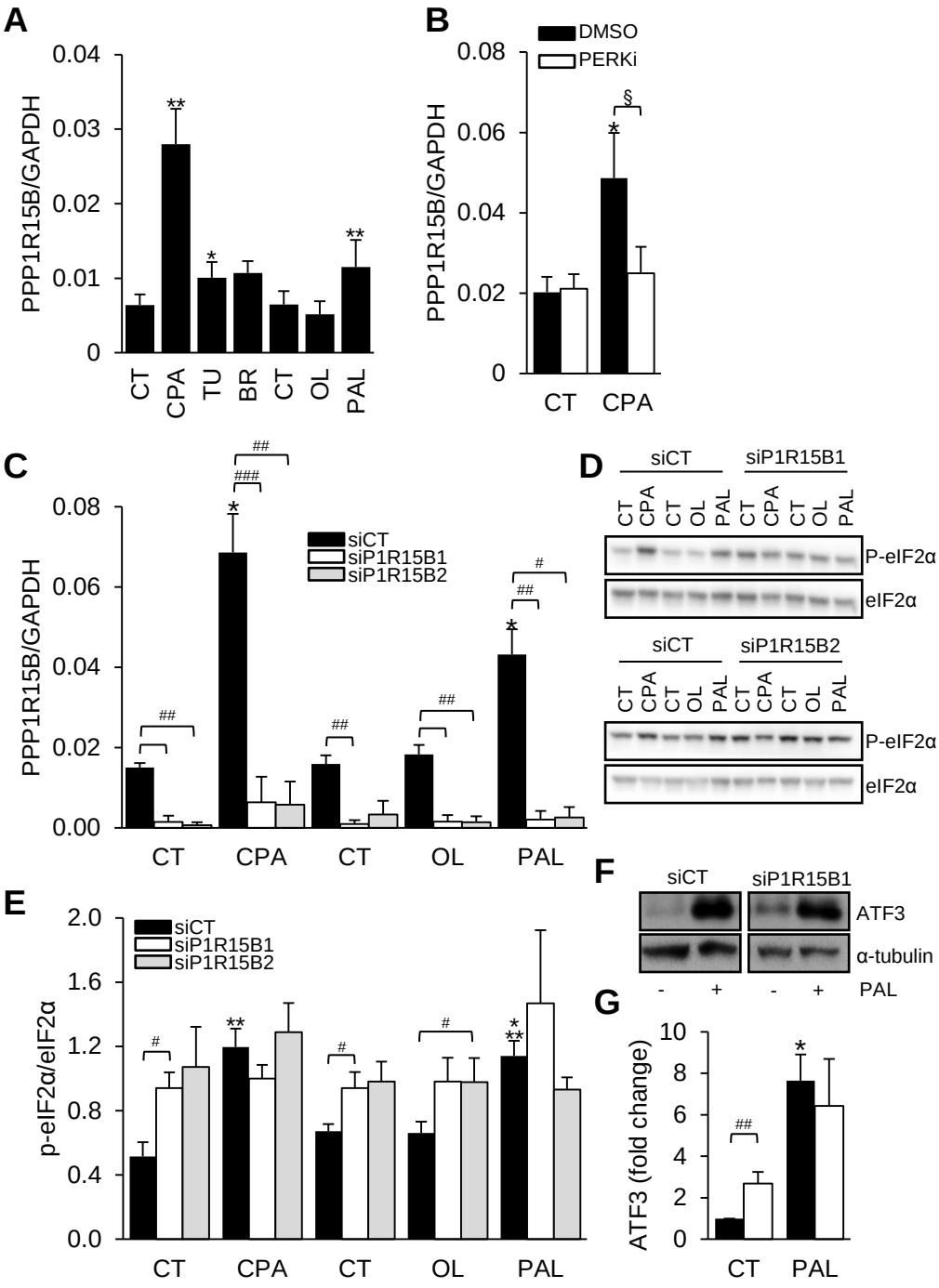
A
PPP1R15B/GAPDH
0.04
0.03
0.02
0.01
0
CT
CPA
TU
BR
CT
OL
PAL
B
DMSO
PERKi
PPP1R15B/GAPDH
0.08
0.06
0.04
0.02
0
CT
CPA
C
PPP1R15B/GAPDH
siCT
siP1R15B1
siP1R15B2
CT
CPA
CT
OL
PAL
D
siCT
siP1R15B1
siP1R15B2
P-eIF2α
eIF2α
E
p-eIF2α/eIF2α
siCT
siP1R15B1
siP1R15B2
F
siCT
siP1R15B1
ATF3
α-tubulin
PAL
G
ATF3 (fold change)
CT
PAL

Figure 5

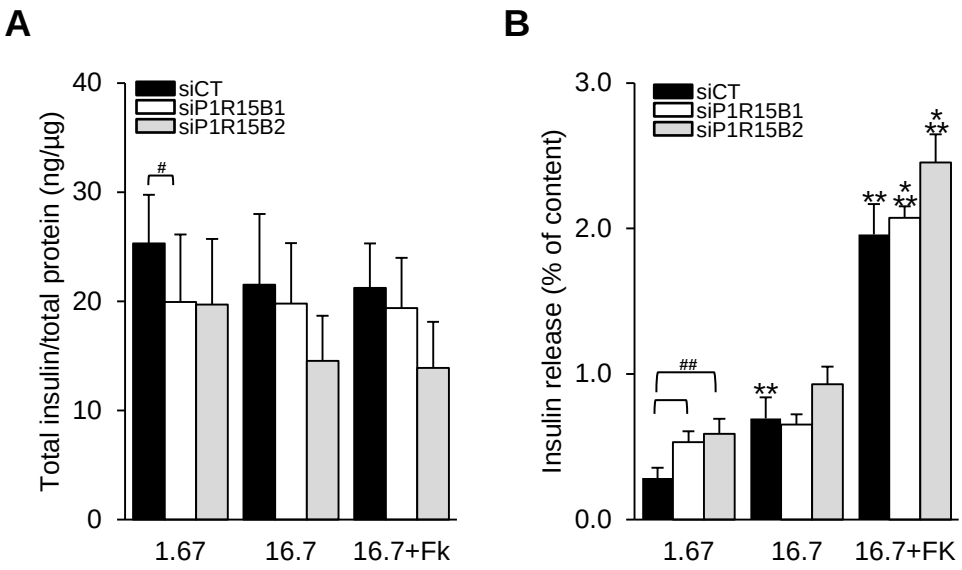
A
B
siCT
siP1R15B1
siP1R15B2
Total insulin/total protein (ng/µg)
Insulin release (% of content)
1.67
16.7
16.7+Fk
16.7+FK
#
##
**
*

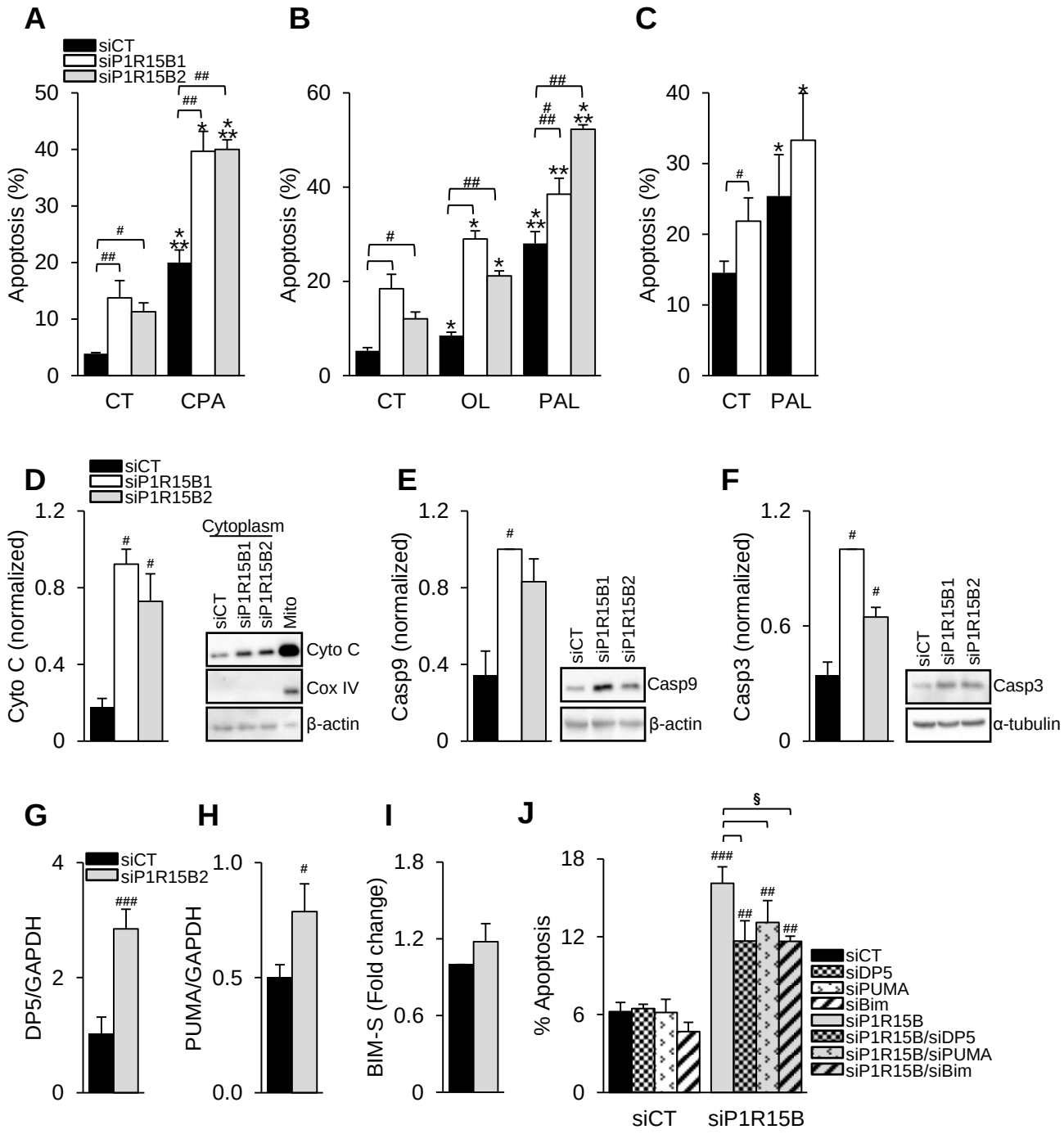
A
siCT
siP1R15B1
siP1R15B2
Apoptosis (%)
CT
CPA
B
Apoptosis (%)
CT
OL
PAL
C
Apoptosis (%)
CT
PAL
D
siCT
siP1R15B1
siP1R15B2
Cyto C (normalized)
Cytoplasm
siCT
siP1R15B1
siP1R15B2
Mito
Cyto C
Cox IV
β-actin
E
Casp9 (normalized)
siCT
siP1R15B1
siP1R15B2
Casp9
β-actin
F
Casp3 (normalized)
siCT
siP1R15B1
siP1R15B2
Casp3
α-tubulin
G
siCT
siP1R15B2
DP5/GAPDH
H
PUMA/GAPDH
I
BIM-S (Fold change)
J
% Apoptosis
siCT
siP1R15B
siCT
siDP5
siPUMA
siBim
siP1R15B
siP1R15B/siDP5
siP1R15B/siPUMA
siP1R15B/siBim

SUPPLEMENTARY DATA

Supplementary Table 1: PCR amplification and sequencing primers used for Sanger sequencing of human *PPP1R15B* gene

Region amplified	Chromosome 1 map position[a]		PCR amplification and sequencing primer (5'-3')			Product Size (bp)
	Start	End	Forward	Reverse	Internal sequencing primers	
Promoter	204380800	204381633	CTCGACGCTTCAACACCA	GGGCATTCAACCTTCCAT		834
Exon 1	204380426	204381021	CGTCGGGAACTTAGAAGAGC	GACGTAGACGCCCAACAGTC		596
Exon 1	204379845	204380621	GGAAAGCAGTCCAGGTAGGA	TCTGTAGGCTTCCTCCGAAT		777
Exon 1	204379186	204379984	CTTCCTCATCCCAATCCTCA	TTGCCCAGTAGCCTTCAATC		799
Exon 1	204378537	204379351	AAGCCTCCAAAGTCATGCTG	GGAGAGGGCCGAATAAGTGT		815
Intron[b]	204376192	204377016	AATAACCACTATATCCCTGGAAGTC	CCTTTGACTACCTGCCATTG		825
Exon 2	204375199	204375499	CTAGGACTACAGGCTGCCAAC	CCTCAATGCTGATTGTAAGATCC		301
Exon 2	204374565	204375305	TTGTGGCAGTCCTTGGAAAT	GCTTGACATTTGAACACAGAGA		741
Exon 2	204374234	204374967	TGACAGTGCTGAGGCATGAT	ATGTCCTTTGCCTGCATGA		734
Exon 2	204373791	204374484	CCCTGTAAGCACTTCTGATGA	TTTGAAGAGGGTTCTGTGTACG		694
Exon 2	204372956	204373998	TCCTTTCTGTCCTTCTTATCACC	GCATTGACTGTTTGTGTTTGG	CAGCTTGGAGTGCAGTGG	1043
Exon 2	204372325	204373064	AAAGCTAGGGCCAATTTCAG	TGGGATTCTAACCTCACTACCAA		740

[a]Map position on hg19 reference sequence. [b]This intronic region was selected as potentially functionally relevant to PPP1R15B because it shows species conservation and includes non-spliced human ESTs.

Supplementary Table 2: siRNA sequences

siRNA	Sequence	Company	Validated in
P1R15B 1	GACUUACUGUUGUACAGCATT	Invitrogen	
P1R15B 2	AAGGGAUGGAUGCAGGUUCCA		(1)
DP5	UCACAGUUUCUUGGUGCUAAGUGUA	Invitrogen	(2)
PUMA	ACGAGCGGCGGAGACAAGAAGAGCA	Invitrogen	(3)
Bim	CGAGGAGGGCGUUUGCAAACGAUUA	Invitrogen	(3)

Supplementary Table 3: Primer sequences used for mRNA expression studies

Gene	STD/RT[a]	Forward	Reverse	Size
PPP1R15B	STD	AGGCAGTCAGGCATCCTCT	TCAAGTAAGAGATGGAGTGGG	431
	RT	TGGGTGAGGCACTTTCTGG	TGGCGACTTCTGTTTCCTG	177
GAPDH	STD	ATGACTCTACCCACGGCAA	TGTGAGGGAGATGCTCAGTG	930
	RT	AGTTCAACGGCACAGTCAA	TACTCAGCACCAGCATCACC	136
DP5	STD	GCACCCTGTGACCTTCCTA	TCACATGCACGAACACACAC	550
	RT	GCCGTGGTGTTACTTGGAC	GATTGTGCCAGAGCTTCACA	125
PUMA	STD	TGGGTGCACTGATGGAGA	AACCTATGCAATGGGATGGA	497
	RT	AGTGCGCCTTCACTTTGG	CAGGAGGCTAGTGGTCAGGT	109

[a] STD: Standard, RT: Real time

Supplementary Table 4: Filtering of variants identified by whole exome sequencing of patient 1 (index patient)

Filter	Patient 1
All variants	55298
Homozygous variants[a]	19591
Coding-affecting variants[b]	3934
Rare Variants[c]	18

Counts are the number of autosomal variants (SNVs and insertion/deletion variants (indels)) identified by Whole Exome Sequencing of the patient compared to the Human Reference Genome on UCSC build hg19. The successive filters applied after quality filtering are shown: [a]homozygous variants, [b]nonsynonymous variants including missense and nonsense, splice-site variants and exonic indels (frameshift and non-shifted), [c]variants that were absent in the homozygous status in an in-house database, in Exome Variant Server (EVS) and in Exome Aggregation Consortium (ExAC) and with a MAF < 0.005 in these databases and in dbSNP.

Supplementary Table 5: Description of the 18 rare variants identified by whole exome sequencing in patient 1, and complementary genotyping of these variants in patient 2

Map position	Gene	cDNA RefSeq	cDNA change	Protein RefSeq	Protein change	rs number	EVS heterozygous count/total (frequency)	EVS MAF	ExAC heterozygous count/total (frequency)	ExAC MAF	Genotype Patients 1	2
chr1:150532595G>A	**ADAMTSL4**	**NM_019032**	**c.3384G>A**	**NP_061905**	**p.Val1050Ile**	**rs201941243**	**Absent**	**0**	**9/60664 (0.00015)**	**0.00007**	**2/2**	**2/2**
chr1:152285138A>G	**FLG**	**NM_002016**	**c.2262T>C**	**NP_002007**	**p.Ser742Pro**	**NA**	**Absent**	**0**	**2/60705 (0.00003)**	**0.00002**	**2/2**	**2/2**
chr1:200972760C>A	**KIF21B**	**NM_017596**	**c.1485G>T**	**NP_060066**	**p.Arg389Leu**	**NA**	**Absent**	**0**	**Absent**	**0**	**2/2**	**2/2**
chr1:204375390G>A	**PPP1R15B**	**NM_032833**	**c.2379C>T**	**NP_116222**	**p.Arg658Cys**	**NA**	**Absent**	**0**	**Absent**	**0**	**2/2**	**2/2**
chr1:205632155G>A	**SLC45A3**	**NM_033102**	**c.1105C>T**	**NP_149093**	**p.Ala255Val**	**rs142713511**	**3/6492 (0.00046)**	**0.00023**	**19/57327 (0.00033)**	**0.00017**	**2/2**	**2/2**
chr10:79601934T>C	DLG5	NM_004747	c.1214A>G	NP_004738	p.His381Arg	rs150885638	9/6503 (0.0014)	0.00069	68/60227 (0.0011)	0.00056	2/2	1/2
chr11:6646598C>T	DCHS1	NM_003737	c.7380G>A	NP_003728	p.Arg2326His	NA	Absent	0	1/60150 (0.00002)	0.00001	2/2	1/2
chr16:1719068C>T	CRAMP1L	NM_020825	c.3401C>T	NP_065876	p.Pro1134Leu	NA	Absent	0	2/55044 (0.00004)	0.00002	2/2	1/2
chr16:1967936T>C	HS3ST6	NM_001009606	c.298A>G	NP_001009606	p.Thryr99Cys	NA	Absent	0	Absent	0	2/2	1/2
chr16:2816615 G>A	SRRM2	NM_016333	c.6635G>A	NP_057417	p.Arg2029His	NA	Absent	0	6/60547 (0.00010)	0.00005	2/2	1/2
chr18:8784555C>T	MTCL1	NM_015210	c.1587C>T	NP_056025	p.Ala482Val	rs115077293	13/6502 (0.0020)	0	57/56978 (0.0010)	0.00050	2/2	1/2
chr19:2807595C>T	THOP1	NM_003249	c.1197C>T	NP_003240	p.Arg348Cys	NA	Absent	0	3/58471 (0.00005)	0.00003	2/2	1/2
chr19:2851553C>T	ZNF555	NM_152791	c.356C>T	NP_001166246	p.Thr73Met	rs369544612	2/6503 (0.00031)	0	8/60476 (0.00013)	0.00007	2/2	1/2
chr2:210742714G>C	**UNC80**	**NM_032504**	**c.3963G>C**	**NP_115893**	**p.Glu1295Gln**	**rs187089611**	**Absent**	**0**	**4/10840 (0.00037)**	**0.00018**	**2/2**	**2/2**
chr3:133474254A>G	TF	NM_001063	c.858A>G	NP_001054	p.Thr184Ala	rs139768770	3/6503 (0.00046)	0.00023	14/60704 (0.00023)	0.00012	2/2	1/2
chr3:133647257A>G	C3orf36	NM_025041	c.1402T>C	NP_079317	p.Ser131Pro	rs149002991	1/6503 (0.00015)	0.00008	4/60232 (0.00007)	0.00003	2/2	1/2
chr5 :169310284C>A	FAM196B	NM_001129891	c.2003G>T	NP_001123363	p.Asp207Tyr	rs200832892	Absent	0	15/10832 (0.0014)	0.00069	2/2	1/2
chr8 :23560457A>G	NKX2-6	NM_001136271	c.226T>C	NP_001129743	p.Leu56Pro	NA	Absent	0	Absent	0	2/2	1/2

Genomic map position is on UCSC hg19. Description of the consequences on cDNA and protein follows the Human Genome Variation Society (HGVS) recommendations (4). Heterozygotes and total genotype counts, heterozygotes frequencies, and minor allele frequencies (MAF) are given for EVS and ExAC. All the variants were absent in the homozygous status in these databases. The genotype of the two affected siblings is shown as 2/2 (homozygous for the rare allele), 1/2 (heterozygous) and 1/1 (homozygous for the frequent allele, none found). Variants homozygous in both patients are shown in bold. NA: not available.

Supplementary Table 6: Functional predictions of the variants compatible with mutation status and human mutations and knockout mouse phenotypes of the corresponding genes

Gene	Name	Protein RefSeq	Protein change	Polyphen (score)	Provean (score)	SIFT (score)	Monogenic disease (mode of inheritance)	Knockout mouse model (homozygous)	Human islet expression (RPKM)[a]
ADAMTSL4	ADAMTS-like 4	NP_061905	p.Val1050Ile	Probably damaging (1)	Neutral (-0.69)	Damaging (0.014)	Ectopia lentis (autosomal recessive) (5)	NA	1.6
FLG	filaggrin	NP_002007	p.Ser742Pro	Benign (0.018)	Neutral (-1.77)	Tolerated (0.201)	Atopic dermatitis, ichtyosis vulgaris (semi-dominant) (6)	Atopic dermatitis (7)	0.9
KIF21B	kinesin family member 21B	NP_060066	p.Arg389Leu	Probably damaging (0.998)	Deleterious (-6.29)	Damaging (0.001)	Not reported	Cellular phenoype : chromosome instability[a]	0.7
PPP1R15B	protein phosphatase 1, regulatory subunit 15B	NP_116222	p.Arg658Cys	Probably damaging (1)	Deleterious (-7.48)	Damaging (0.000)	Not reported	Post-natal lethal, extremely small size (4)	12.1
SLC45A3	solute carrier family 45, member 3	NP_149093	p.Ala255Val	Benign (0.015)	Neutral (-1.11)	Tolerated (0.169)	Not reported	NA	3.1
UNC80	Ung-80 homolog (C. elegans)	NP_115893	p.Glu1295Gln	Possibly damaging (0.844)	Neutral (-1.61)	Damaging (0.041)	Not reported	NA	7.9

In silico prediction of the impact and severity of mutation on protein function was performed using Polyphen-2 (8), SIFT and Provean (9), using recommended parameters. Polyphen-2 predictions were made based on the HumDiv model. [a]Human islet expression is based on (10) and our unpublished data (M.C.) and is given in RPKM (reads per kilobase of exon model per million mapped reads) units. [b]Knockout mouse model phenotype information is according to the Mouse Genome informatics (MGI) and the Wellcome Trust Sanger Institute (WTSI) databases. NA: not available.

Supplementary Figure 1: Heatmap of gene expression in human tissues. RNAseq values (in RPKM) from the indicated human tissues were obtained from GTEx (v4.p1). RNA-seq data of FACS-purified human islet β-cells were from Nica et al (11). Human islet RNA-seq data (24 in total) were from Eizirik et al and Cnop et al (10;12) (and unpublished data). Bone (osteoblast) gene expression was obtained from GEO dataset accession number GSE57925 (unpublished data). The median RPKM value of the samples is represented, with the maximum set at 30. The heatmap was made in R (function heatmap.2).

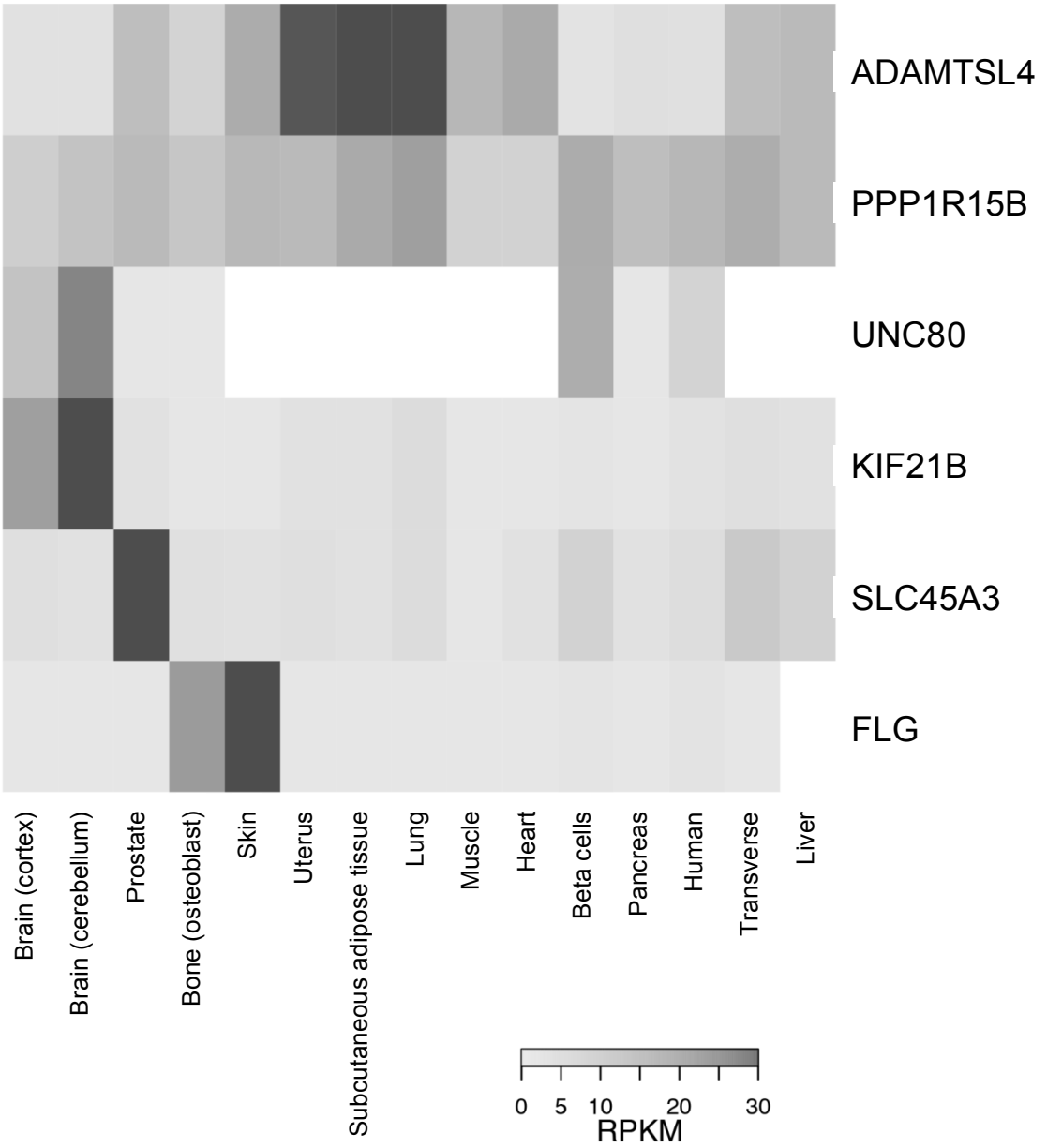

Supplementary Figure 2: **PPP1R15B silencing does not modify expression of the pro-apoptotic Bim splice variants Bim-EL and Bim-L or the anti-apoptotic proteins BCL2 and BCL-XL.** INS-1E cells were transfected with control siRNA (siCT) or two different siRNAs targeting PPP1R15B (siP1R15B1 and siP1R15B2). 48h after transfection the Bim-EL and Bim-L (A, B, C) and BCL2 and BCL-XL (D, E, F) expression was examined by Western blot. A and D are representative blots of 5 experiments. B, C, E and F are densitometric quantifications of protein expression corrected for α-tubulin, and expressed as fold of siCT.

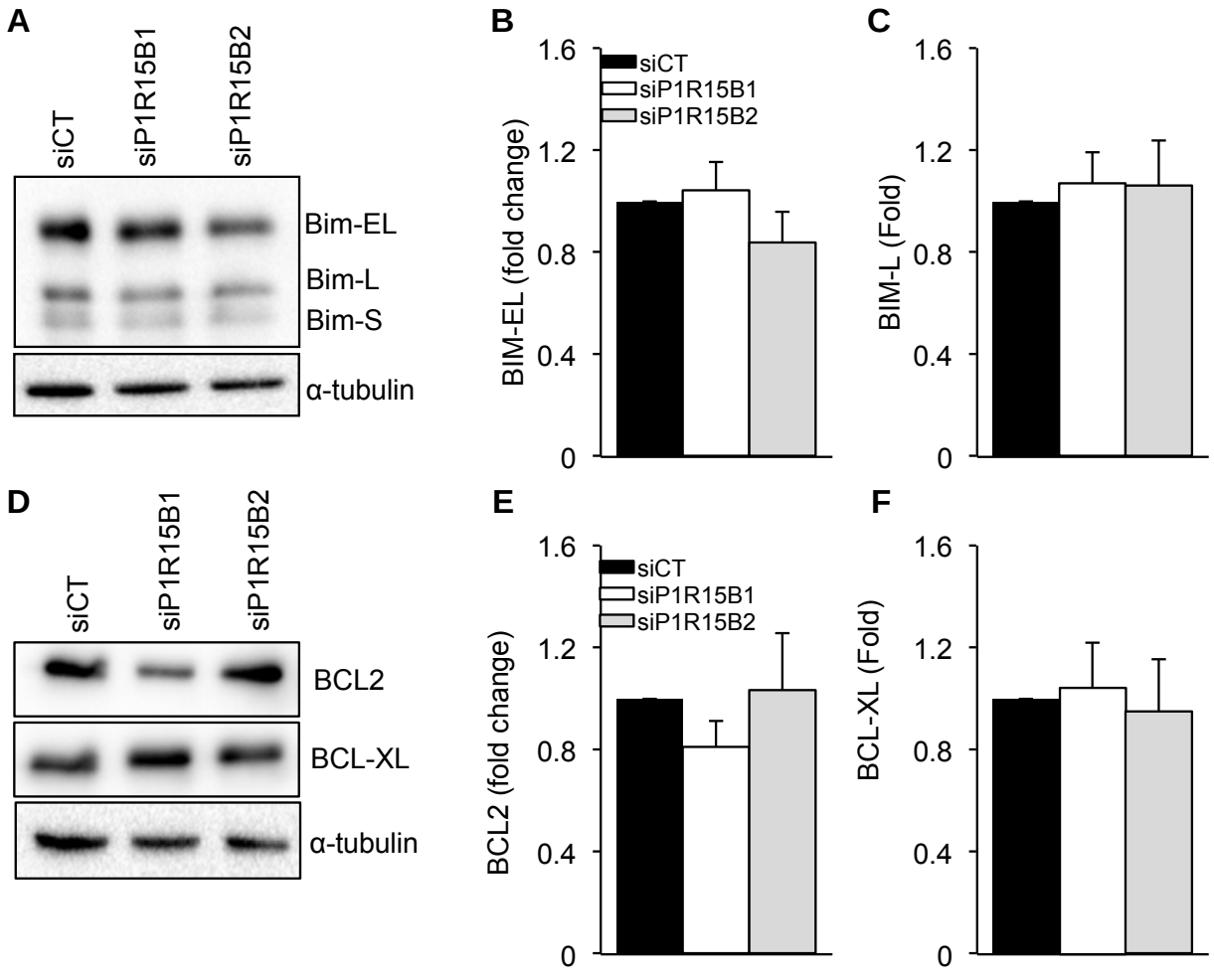

Supplementary References

1. Jousse C, Oyadomari S, Novoa I, Lu P, Zhang Y, Harding HP, Ron D. Inhibition of a constitutive translation initiation factor 2α phosphatase, CReP, promotes survival of stressed cells. J Cell Biol 2003;163:767-775
2. Cunha DA, Igoillo-Esteve M, Gurzov EN, Germano CM, Naamane N, Marhfour I, Fukaya M, Vanderwinden JM, Gysemans C, Mathieu C, Marselli L, Marchetti P, Harding HP, Ron D, Eizirik DL, Cnop M. Death protein 5 and p53-upregulated modulator of apoptosis mediate the endoplasmic reticulum stress-mitochondrial dialog triggering lipotoxic rodent and human β-cell apoptosis. Diabetes 2012;61:2763-2775
3. Gurzov EN, Germano CM, Cunha DA, Ortis F, Vanderwinden JM, Marchetti P, Zhang L, Eizirik DL. p53 up-regulated modulator of apoptosis (PUMA) activation contributes to pancreatic beta-cell apoptosis induced by proinflammatory cytokines and endoplasmic reticulum stress. J Biol Chem 2010;285:19910-19920
4. Harding HP, Zhang Y, Scheuner D, Chen JJ, Kaufman RJ, Ron D. Ppp1r15 gene knockout reveals an essential role for translation initiation factor 2 alpha (eIF2alpha) dephosphorylation in mammalian development. Proc Natl Acad Sci U S A 2009;106:1832-1837
5. Ahram D, Sato TS, Kohilan A, Tayeh M, Chen S, Leal S, Al-Salem M, El-Shanti H. A homozygous mutation in ADAMTSL4 causes autosomal-recessive isolated ectopia lentis. Am J Hum Genet 2009;84:274-278
6. Palmer CN, Irvine AD, Terron-Kwiatkowski A, Zhao Y, Liao H, Lee SP, Goudie DR, Sandilands A, Campbell LE, Smith FJ, O'Regan GM, Watson RM, Cecil JE, Bale SJ, Compton JG, DiGiovanna JJ, Fleckman P, Lewis-Jones S, Arseculeratne G, Sergeant A, Munro CS, El HB, McElreavey K, Halkjaer LB, Bisgaard H, Mukhopadhyay S, McLean WH. Common loss-of-function variants of the epidermal barrier protein filaggrin are a major predisposing factor for atopic dermatitis. Nat Genet 2006;38:441-446
7. Kypriotou M, Boechat C, Huber M, Hohl D. Spontaneous atopic dermatitis-like symptoms in a/a ma ft/ma ft/J flaky tail mice appear early after birth. PLoS One 2013;8:e67869
8. Adzhubei IA, Schmidt S, Peshkin L, Ramensky VE, Gerasimova A, Bork P, Kondrashov AS, Sunyaev SR. A method and server for predicting damaging missense mutations. Nat Methods 2010;7:248-249
9. Choi Y, Sims GE, Murphy S, Miller JR, Chan AP. Predicting the functional effect of amino acid substitutions and indels. PLoS One 2012;7:e46688
10. Cnop M, Abdulkarim B, Bottu G, Cunha DA, Igoillo-Esteve M, Masini M, Turatsinze JV, Griebel T, Villate O, Santin I, Bugliani M, Ladriere L, Marselli L, McCarthy MI, Marchetti P, Sammeth M, Eizirik DL. RNA sequencing identifies dysregulation of the human pancreatic islet transcriptome by the saturated fatty acid palmitate. Diabetes 2014;63:1978-1993
11. Nica AC, Ongen H, Irminger JC, Bosco D, Berney T, Antonarakis SE, Halban PA, Dermitzakis ET. Cell-type, allelic, and genetic signatures in the human pancreatic beta cell transcriptome. Genome Res 2013;23:1554-1562
12. Eizirik DL, Sammeth M, Bouckenooghe T, Bottu G, Sisino G, Igoillo-Esteve M, Ortis F, Santin I, Colli ML, Barthson J, Bouwens L, Hughes L, Gregory L, Lunter G, Marselli L, Marchetti P, McCarthy MI, Cnop M. The human pancreatic islet transcriptome: expression of candidate genes for type 1 diabetes and the impact of pro-inflammatory cytokines. PLoS Genet 2012;8:e1002552